Application of Raman Spectroscopy to Real-Time Monitoring of CO2 Capture at PACT pilot Plant; Part 1: Plant operational data

Highlights:

- Raman spectroscopy is employed for real time monitoring of CO_2 capture plant
- A multivariate regression model was used to determine rich and lean CO_2 loadings
- Reliability of the Raman predictions are confirmed with the titration measurements
- The Raman predictions models are not affected with accelerated solvent degradation caused by high conc. of SO_2
- It is demonstrated that the technology is a step closer to making offline measurements a thing of the past and moving towards predictive control of CO_2 capture plants

Application of Raman Spectroscopy to Real-Time Monitoring of CO_2 Capture at PACT pilot Plant; Part 1: Plant operational data

Muhammad Akram[a,] M.H. Wathsala N. Jinadasa[b], Paul Tait[c] Mathieu Lucquiaud[c], Kris Milkowski[a], Janos Szuhanszki[a], Klaus-Joachim Jens[b], Maths Halstensen[b], Mohammed Pourkashanian[a],*

[a]The University of Sheffield, United Kingdom
[b]University of South-eastern Norway, Norway
[c]The University of Edinburgh, United Kingdom

[*]Corresponding author: m.akram@sheffield.ac.uk
Energy2050,Energy Engineering Group, Department of Mechanical Engineering, Ella Armitage Building, University of Sheffield, Sheffield S3 7RD,UK

ABSTRACT

Process analyzers for in-situ monitoring give advantages over the traditional analytical methods such as their fast response, multi-chemical information from a single measurement unit, minimal errors in sample handing and ability to use for process control. This study discusses the suitability of Raman spectroscopy as a process analytical tool for in-situ monitoring of CO_2 capture using aqueous monoethanolamine (MEA) solution by presenting its performance during a 3-day test campaign at PACT pilot plant in Sheffield, UK. Two Raman immersion probes were installed on lean and rich streams for real time measurements. A multivariate regression model was used to determine the CO_2 loading. The plant performance is described in detail by comparing the CO_2 loading in each solvent stream at different process conditions. The study shows that the predicted CO_2 loading recorded an acceptable agreement with the offline measurements. The findings from this study suggest that Raman Spectroscopy has the capability to follow changes in process variables and can be employed for real time monitoring and control of the CO_2 capture process. In addition, these predictions can be used to optimize process parameters; to generate data to use as inputs for thermodynamic models, plant design and scale-up scenarios.

Keywords : CO_2 capture, Raman spectroscopy, in-situ process monitoring

1. Introduction

Carbon Capture, Utilisation and Storage (CCUS) is gaining highlights due to its potential to tackle the climate change problem. The UK Government's "Clean Growth Strategy" highlights the role of CCUS in reducing greenhouse gas emissions alongside other options i.e. the need for switching from fossils to low carbon fuels (Clean Growth, 2018). Although the technology is expensive at the moment, it has the potential to provide deep and affordable CO_2 emission reductions from coal and gas-fired power generation. The technologies to meet greenhouse gas emission limits will cost double if no CCUS is used (BEIS report, 2019). There are many technological options being considered for CCUS but post combustion capture using alkanolamine solutions is by far the most understood process due its long time use in the process industry. Although this process has been applied in the oil and gas industry for many decades (Polasek and Bullin, 2006), it has been predominantly applied to clean gases. Its application to

power plant and industrial flue gases, which may have contaminants, is relatively new and is in the early phase of commercial deployment. Sask Power (Boundary Dam 3) in Canada and Petra Nova in USA are two example of commercial deployment of this versatile technology. There are also a number of research facilities in industrial and academic setups working on different aspects of the technology (de Cazenove et al. 2016; Akram et al. 2016; Notz et al. 2012; Mejdell et al. 2011).

Several research work is carried on developing and optimizing methods to remove CO_2 from power plants and industrial sources using amine technology. Process modifications (Kang et al. 2016; Jassim et al. 2007; Le Moullec et al. 2014; Madan et al. 2013; Ahn et al. 2013; Amrollahi et al. 2011; Oh et al. 2018; Diego et al. 2017; Merkel et al. 2013; Herraiz, 2016) and new solvents (Aronu et al. 2010; Kumar et al. 2014; Hakka 2007; Yuan and Rochelle, 2018; Wang et al. 2015; Yang et al. 2016; Kim et al. 2013; Cheng et al. 2013; Abu Zahra et al. 2007) are being tested to minimise these issues. The process is complex and is greatly affected by process parameters. Moreover, the presence of oxygen and other impurities such as NO_x and SO_x in the flue gases cause solvent degradation. Degraded solvent results in reduced process performance. Inline solvent monitoring is essential for real-time evaluation of the plant performance and assessing solvent quality. Moreover, it is an important aspect from solvent management point of view and in order to control the process at optimum conditions. However, a well-established method for this purpose is currently not available.

The chemical process of CO_2 absorption by aqueous MEA solutions are attributed by a number of parameters including CO_2 loading (mol_{CO2}/mol_{MEA}) and solvent concentration. The CO_2 loading in an absorption process is also an indication of the carbon species-products that exist as a result of the reaction between CO_2 with amine while in a desorption process it expresses the efficiency of desorption and degree of regeneration of the solvent for the recirculation to the absorption column for further CO_2 capture from flue gas. Solvent concentration can vary during the process due to evaporative and degradation losses. The solvent concentration has to be maintained for optimum operation of CO_2 capture plants. Therefore these two parameters are frequently tested during plant operations to characterize both absorption and desorption while a detailed analysis of all the chemical components in the solvent stream is important to understand chemical mechanisms and reaction kinetics. It is apparent that a real-time measurement represents actual plant operation more realistically than a periodical monitoring method which only gives measurements in different time intervals where the non-measured points are predicted based on the trend which can lead to either over-predictions or under-predictions. Unavailability of real-time measurements results in lack of process control. The CO_2 capture process by amines needed to be improved and optimized, to reduce the capital and operational cost and find solutions for amine degradation and corrosion problems. Availability of a real-time monitoring method will provide increased process understanding and possible routes of continuous improvement in a faster and more reliable way. In addition, real-time monitoring helps for making more data-driven decisions.

Few developments are published in real-time monitoring methods of CO_2 capture process. Monitoring of CO_2 capture by aqueous AMP-PZ system and MDEA-PZ high pressure system are reported by TNO group, Netherlands using chemometrics approach and pilot plant demonstration. They predicted the concentrations of MDEA, PZ, and CO_2 using real-time measurements of solvent properties which were density, pH, conductivity, sound velocity, refractive index and NIR absorption (Kachko *et al.*, 2016a). A similar approach was used to predict AMP, PZ and CO_2 in another pilot plant test (Kachko et al., 2015). During long term pilot demonstrations at TCM CO_2 capture pilot plant in Norway, CO_2 loadings and solvent concentration were mainly followed on a daily basis with manual samples and analysis and they

also used online analyzers such as conductivity, density and pH to make correlations to CO_2 loading and solvent strength (Andersson *et al.*, 2013; Flø *et al.*, 2017; Montañés *et al.*, 2017). Due to the long term use and proven reliability, and familiarity with wet chemical methods, offline analysis are still used such as barium chloride ($BaCl_2$) titration-precipitation method (Idris *et al.*, 2014; Weiland *et al.*, 1969) and analysis via acidic evolution (Hilliard, 2008) and LC-MS (Knudsen *et al.*, 2014) for determining CO_2 loadings.

Raman spectroscopy is one of in-situ monitoring tools in manufacturing industry. It gives unique data based on the Raman scattered light by laser induced molecular vibrations. It provides a high information content about a chemical system, faster measurements within few seconds, no sample preparation is required and easy to use in plant applications. A method for in situ specie distribution of a CO_2 loaded alkanolamine solution by Raman spectroscopy was proposed by (Souchon *et al.*, 2011) and (Vogt *et al.*, 2011) showed how CO_2 loading can be qualitatively interpreted from Raman spectra. A complete carbon and amine specie distribution was presented by (Wong *et al.*, 2015, 2016). Samarakoon *et al.*, (2013) proposed a method to determine carbon species in a CO_2 loaded MEA solution by calculating molar scattering factor while (Idris *et al.*, 2014) used area under a Raman peak to develop calibration curves. Raman spectroscopy for real-time quantitative analysis was demonstrated in a laboratory rig operation for MEA solvent by Jinadasa *et al.*, (2017). A comparison of Raman method with infrared spectroscopy was presented by Puxty *et al.*, (2016) while Kachko *et al.*, (2016b) compared Raman, near infrared, and Fourier-transform infrared for in-line monitoring of CO_2 capture plants. The above cited literature reveals the capability of Raman method for monitoring the concentration profiles in real-time applications.

There is not much published data on the use of Raman Spectroscopy as a real time plant monitoring and optimization tool. This study supports the use of this technique in two aspects. Firstly, it demonstrates the reliability of the spectroscopic method for faster and precise measurements in a variety of process conditions by comparing the Raman measurements with standard offline analytical results. Secondly, it provides evidence for the response of CO_2 absorption and desorption process on steady and dynamic process conditions and its sensitivity thus proving the capability of Raman spectroscopy to be used as a tool to increase process understanding, optimization and control. Trials for this study were performed as a three day-campaign at UKCCSRC Pilot-scale Advanced CO_2 Capture Technology (PACT) Facility, Sheffield, UK. The trends in key plant variables capture efficiency, temperature profiles and emission measurements are presented and discussed with respect to Raman measurements. To the author's knowledge, in open literature, no one has analyzed the capture process performance with parametric changes in relation to Raman Spectroscopy measurements in as detail as presented in this paper.

A Raman measurement is a spectrum which shows the Raman scattering intensity as a function of the frequency shifts. This intensity depends on the vibrational, rotational and other low frequency transitions in molecules when excited by a laser. Calibration is required to convert the indirect Raman measurement into a useful information such as a concentration of chemical specie in a system. There are two types of calibration approaches which are univariate analysis and multivariate analysis. A chemometric based multivariate approach was used in this study to convert raw Raman spectra into concentration values because this method is more robust than the traditional univariate analysis (Esbensen, 2010). The process of instrument calibration to fit for a plant operation is an extensive process and therefore is presented as the second part

of this paper in a different publication titled as "Raman Spectroscopy for Real-Time Monitoring of CO_2 Capture Process; Part 2: Multivariate Calibration".

2. Methodology

2.1. Description of CO_2 capture pilot plant

The PACT Core Facilities in Sheffield, UK is intended for commercial and academic research enabling users to develop and demonstrate technologies before moving to large-scale trials. A solvent-based carbon capture plant is directly connected to PACT combustion facilities which is capable of capturing one ton of CO_2 per day from an equivalent of approximately 150kW conventional coal combustion flue gas.

A simplified flow diagram of the plant is shown in Figure 1. Specification of the pilot plant used for these tests are given in Table 1. The plant has full absorption and desorption cycle and is equipped with absorber, stripper, reboiler, cross exchanger, carbon filter and water wash. Its gas pre-treatment section can be used either as Flue Gas Desulphurisation (FGD) or Direct Contact Cooler (DCC). The plant has an activated carbon filter to remove some of the degradation products from the solvent. Temperatures of flue gas and lean solvent entering the absorber are controlled. The absorber has 6.5m structured Mellapak CC3 packing while stripper is packed with 7.5m of IMTP25 random packing. Absorber and stripper temperature profile along the height of the columns is measured by 8 and 5 RTDs, respectively. Gas analysis are performed at 5 different locations in the plant. Sampling lines are located at the FGD inlet, absorber inlet, water wash inlet and outlet, and stripper outlet. Gasmet DX4000 FTIR is used for gas analysis which sequentially detects samples from each of the locations. The sequence and sampling time is user defined and can be changed in the FTIR software as and when required. Stripping is performed in the reboiler supplied with pressurized hot water (PHW) generated by electrical heating. The PHW has a bypass to control the flow rate through the reboiler or bypassing it. A pneumatically driven 3-way valve is used for this purpose. The energy used for stripping is calculated by measuring the flow rate, inlet and outlet temperatures of the PHW. Stripper pressure is controlled automatically to a user defined set point. The plant uses two different data logging systems. National Instruments PXi system is used to log most of the data from the plant while Allen Bradly PLC is used to control the plant and log relevant data.

Table 1: Absorber and stripper specifications

Specifications	Absorber	Stripper	Water wash
Diameter (mm)	300	300	300
Packing name	Mellapak CC3	IMTP25	IMTP25
Packing type	Structured	Random	Random
Packing height (m)	6.5	7.5	7.5
Temperature measurements	10	9	-

The Raman spectra were obtained by Kaiser RXN2 multi-channel 785 nm spectrometer with 400mW maximum laser power. Two Raman immersion optic probes (1/4″ diameter, 6″ length, short focused, sapphire window) were directly connected to lean and rich amine process lines at PACT amine plant as shown in Figure 1. iC Raman 4.1 software was used to acquire Raman signals maintaining approximately 1-minute interval during each measurement. Each spectra

were exported to Matlab 2017 for preprocessing. Locations of Raman measurements were selected to reasonably represent lean and rich stream solvent concentrations. Distances from the nearest manual sampling points to the lean and rich Raman probes were 120 cm and 106 cm respectively.

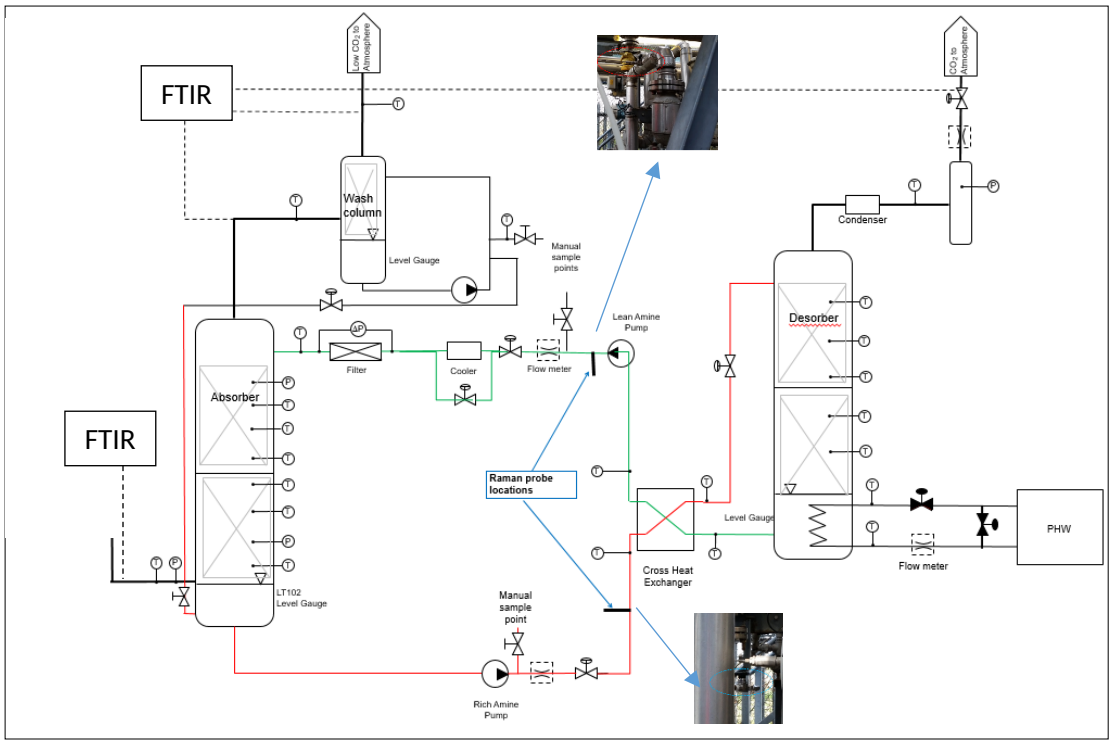

Figure 1: Simplified plant layout with raman probe locations

The accuracy of the real-time predictions were argued by comparing their values with offline liquid sample analysis and their sensitivity to process conditions. Offline liquid analysis were performed to determine CO_2 loading and amine concentration as described in Akram et al. (2016). Mettler Toledo T90 auto-titrator was used to perform acid-base titration where HCl (0.2M) was used to determine total amine concentration and NaOH (0.5M) was used to determine CO_2 concentration. Uncertainties in the titration procedure were determined by preparing a solution of MEA (nominal concentration 29.4%) and loading to 8.04% CO_2 by weight gravimetrically by bubbling CO_2 through it. Three samples from MEA solution thus prepared were then titrated using the titration apparatus to measure MEA concentration and CO_2 loading. The average uncertainty in the loading measurements was found to be +/- 3.15%. This procedure is similar to the previously reported method by Tait *et al.* (2018).

Gas composition was measured by two FTIR instruments, one was used to consistently measure gas composition at the outlet of the absorber, while the other was used to measure gas composition at the inlet of the absorber but was also used to measure at other plant locations from time to time. The gas samples are extracted from the plant using isokinetic sampling probes and routed to the FTIR through heated filters, heated sampling lines and heated cabinet housing solenoid for sample switching. The entire sampling system was heated up to 180 ^{0}C to avoid condensation.

For the first two test campaigns air with CO_2 injection was used as flue gas. During the last test, flue gas from coal combustion was used. The coal flue gas was not passed through FGD so had high concentrations of SO_2. Presence of SO_2 in the flue gas results in faster degradation of solvent. The aim of this tests was to investigate if Raman Spectroscopy measurements are influenced by solvent degradation. The tests were performed with 30% MEA which had been used for 10 days with normal plant operation. The solvent was transparent in appearance by the time of first use.

2.2 Selection of process variable matrix

The tests were divided into three campaigns.

1. Absorption-desorption
2. Process variations
3. Coal flue gas

Details of the three test campaigns are given in the following sections.

2.2.1 Absorption-desorption:

The aim of the absorption-desorption test campaign was to check the accuracy of the predictions by Raman spectroscopy throughout a complete absorption and desorption cycle, and observing whether the two Raman sensors can generate identical results when measuring the same sample. The test was divided into two phases, absorption and desorption, so that during the absorption process there was no desorption and vice versa. The conditions for the test (Tests 1 & 2) are given below, in Table 2.

Table 2: Conditions for absorption-desorption test

Absorption			**Desorption**		
Test 1			Test 2		
Parameter	Value	Unit	Parameter	Value	Unit
Flue gas flow rate	210	m^3/h	Flue gas flow rate	NA	m^3/h
CO_2 concentration	12	v/v%	CO_2 concentration	NA	v/v %
Solvent flow rate	900	kg/h	Solvent flow rate	900	kg/h
Stripper pressure	NA	bar	Stripper pressure	0.6	bar
PHW set point	NA	^0C	PHW set point	128	^0C
PHW flow rate	NA	m^3/h	PHW flow rate	9.8	m^3/h

2.2.2 Process variations:

During these tests, the CO_2 capture plant was operated with full absorption and desorption cycle and the Raman spectroscopy predictions were monitored. Operational conditions, given in Table 3, were varied to investigate the response of Raman instruments against these variations. Solvent flow rate, gas flow rate and CO_2 concentrations were changed. The test was started with around 190 m^3/h gas flow with 5% CO_2 concentration, 600 kg/h solvent flow (Test 3). CO_2 concentration was increased to 12% for the Test 4. Solvent flow rate was increased to 1000 kg/h and 1200 kg/h for the Test 5 and Test 7, respectively. Flue gas flow rate was reduced to 150 m^3/h for the Test 6. Operational data was recorded throughout the test period and manual

samples for rich and lean solvent were collected for bench analysis at 30 minute intervals during this test campaign.

Table 3: conditions for process conditions variation tests

Parameter	Value	Units	Parameter	Value	Units
Test 3			Test 4		
Flue gas flow rate	193	m^3/h	Flue gas flow rate	193	m^3/h
CO_2 concentration	5	v/v %	CO_2 concentration	12	v/v %
Solvent flow rate	600	kg/h	Solvent flow rate	600	kg/h
Stripper pressure	0.4	barg	Stripper pressure	0.4	barg
Test 5			Test 6		
Flue gas flow rate	193	m^3/h	Flue gas flow rate	150	m^3/h
CO_2 concentration	12	v/v %	CO_2 concentration	12	v/v %
Solvent flow rate	1000	kg/h	Solvent flow rate	1000	kg/h
Stripper pressure	0.4	barg	Stripper pressure	0.4	barg
Test 7					
Flue gas flow rate	150	m^3/h	Solvent flow rate	1200	kg/h
CO_2 concentration	12	v/v %	Stripper pressure	0.4	barg

2.2.3 Coal flue gas:

For the first two test campaigns air with CO_2 injection was used as flue gas. The main idea of this test was to investigate if the spectrometer can accurately predict CO_2 loadings if solvent is degraded by the presence of SO_2 in flue gas. For this purpose flue gas from a coal fired combustor was fed to the CO_2 capture plant absorber.

The flue gas was generated by burning bituminous El Cerrejon coal in the 250 kW PACT air/oxy-fired CTF (Combustion Test Facility), operated in air-firing mode. The furnace chamber is cylindrical in shape, 0.9 m in diameter and 4 m long, and it is fitted with a scaled version of a Doosan Babcock Mark III Low-NO_x burner in a down firing arrangement. The flue gas produced was passed through a cyclone and then a high temperature candle filter for particulate removal before a slip stream of it was introduced into the CO_2 capture plant.

The capture plant has a gas pretreatment section which can be employed as FGD for removing Sulphur but for these tests FGD was deliberately not operated in order to send SO_2 to the capture section to accelerate solvent degradation. Carbon filter was also totally bypassed during this test campaign for the same reason. The average concentration of SO_2 in the flue gas entering the absorber was around 210ppm. However, due to short duration of the test, a considerable colour change in the liquid samples, which is an indication of solvent degradation, could not be observed. Conditions for the test are given in Table 4. The following measures were adopted to accelerate solvent degradation.

- Flue gas with 210ppm of SO_2 was fed into the absorber
- Lean solvent temperature was increased to 55 ^{0}C
- Stripper pressure was increased to 0.6 barg to heat up the solvent to a higher temperature
- PHW set point temperature increased to 133 ^{0}C

Due to a plant trip and some sump level instability in the absorber sump, the PHW temperature set point, lean solvent temperature set point and stripper pressure set point were adjusted to 128 ^{0}C, 50 ^{0}C and 0.4 barg, respectively.

Table 4: Test conditions for coal flue gas

Parameter	Value	Units	Parameter	Value	Units
Test 8			Test 9		
Flue gas flow rate	200	m^3/h	Flue gas flow rate	200	m^3/h
CO_2 concentration	12.7	v/v %	CO_2 concentration	12.7	v/v %
SO_2 concentration	210	ppm	SO_2 concentration	210	ppm
Solvent flow rate	1000	kg/h	Solvent flow rate	1000	kg/h
Stripper pressure	0.4	barg	Stripper pressure	0.6	barg
Lean solvent temperature	40	^{0}C	Lean solvent temperature	55	^{0}C
PHW set point	128	^{0}C	PHW set point	133	^{0}C
Test 10					
Flue gas flow rate	200	m^3/h	Solvent flow rate	1000	kg/h
CO_2 concentration	12.7	%	Stripper pressure	0.4	barg
SO_2 concentration	210	ppm	Lean solvent temperature	50	^{0}C
PHW set point	128	^{0}C			

3. Results and Discussion

The results of the three test campaigns are presented in four sections. In section 3.1, real-time Raman predictions are compared with titration measurements. The next three sections discuss the plant trends and how effectively the real-time monitoring tool can correlate to the plant performance during the three test campaigns.

3.1. Raman model predictions with titration measurements

The reaction between CO_2 and MEA is complex and there is still a controversy regarding it's detailed understanding (Xie *et al.*, 2010). However, in Raman spectroscopic point of view, it should be possible to identify the fate of reactants and products according to the behavior of peaks corresponding to Raman active vibrational modes. The reactant-product pool of MEA-CO_2-H_2O system contain carbon ion species as carbonate, bicarbonate, carbamate and amine species as protonated amine and unreacted amine. These chemical species show their identification in different wavelength areas of a Raman spectrum (Jinadasa *et al.*, 2017). The region from 767-1525 cm^{-1} was used to determine the CO_2 loading for the study because this region is rich with vibrational modes related to carbon species. Figure 2 shows Raman spectra obtained during the test with process variations. The raw Raman measurements (Figures 2a, 2b) show different baseline drifts but once they are baseline corrected and scaled, their spectral variations in the fingerprint region become easy to identify the chemical components as can be seen in Figure 2c. The upward arrows in Figure 2 indicate the chemical species (carbonate, bicarbonate, carbamate and protonated amine) as their concentrations increase with increasing CO_2 loading, while the downward arrows point to a vibrational band of free MEA which yields lower concentration as the CO_2 loading is increasing.

The fingerprint area of baseline corrected Raman spectra was used to determine CO_2 loading after applying multivariate calibration approach. The initial regression model development can be found in (Jinadasa, 2019) and the path of how it modified to the PACT plant operation is described in the second part of this paper.

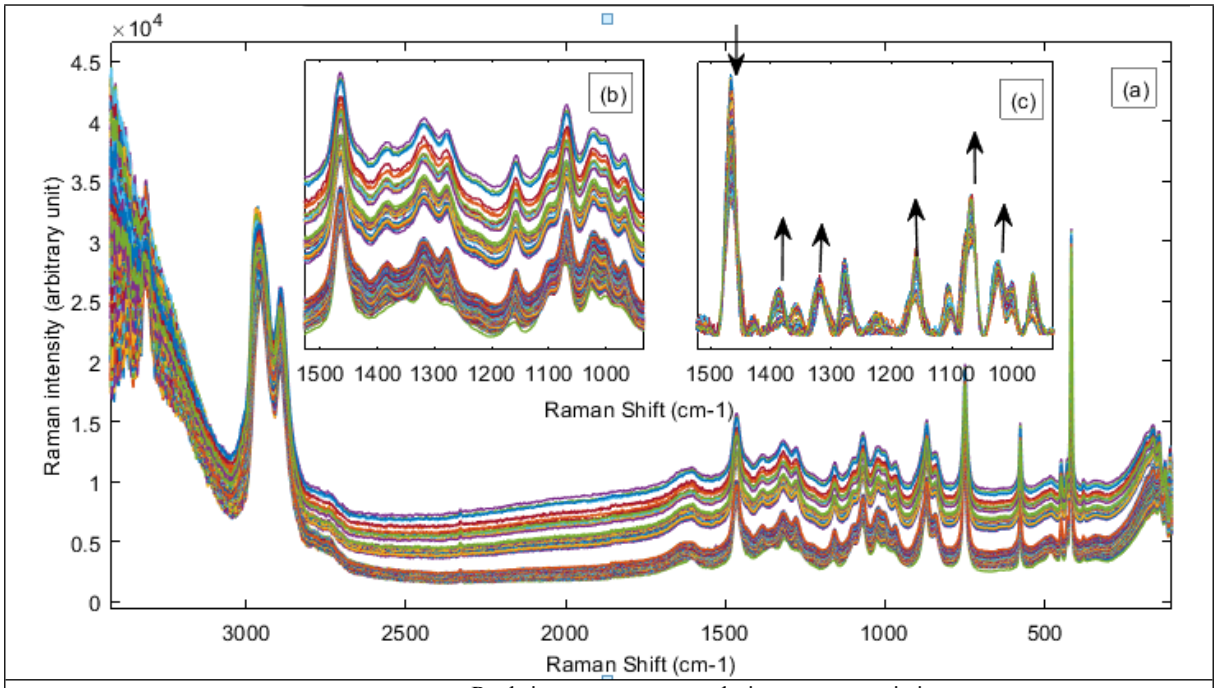

Figure 2. Real-time measurements acquired from Raman probe connected to rich stream during the test campaigns; (a) Raw Raman measurements in the wavelength region 100-3426 cm^{-1} ; (b) Raw Raman measurements in the wavelength region 1000-1500 cm^{-1};(c) Baseline corrected and scaled Raman measurements in the wavelength region 1000-1500 cm^{-1} ; arrows in the plot (c) indicate Raman intensities of vibrational bands related to different species present in the system which vary according to different CO_2 loading values –arrow up: increasing intensity with increasing CO_2 loading; arrow down = decreasing intensity with increasing CO_2 loading

3.2 Campaign 1 – Absorption and desorption

The campaign was divided into two separate tests, one each for absorption and desorption. This section presents results of the absorption and desorption tests, separately. In order to avoid confusion, it is essential to clarify here that rich loading refers to the measurement at the outlet of the absorber and lean loading refers to the measurement at the outlet of the reboiler, regardless of whether the absorption/desorption process was in operation or not.

Please note that for these tests steady state conditions were not achieved as there was no stripping during absorption and vice versa. Steady state is normally defined by the steady CO_2 concentrations at the absorber outlet. However, it was not possible to achieve this condition during these tests.

3.2.1. Absorption:

Conditions for this test were, 900 kg/h solvent flow and 210 m^3/h flue gas with 12% CO_2. To calculate real time CO_2 capture efficiency, two FTIR instruments, at the inlet and outlet of the absorber, were used to measure CO_2 concentration in the flue gas. The plant was operated in absorption mode until the CO_2 concentration in the flue gas leaving the absorber was almost

306 equal to that entering the absorber, which indicated that the solvent was approaching its
307 maximum CO_2 loading under the conditions of the test.

308 During absorption, there was no supply of PHW to the reboiler so the absorber was the only
309 location where process changes happened. Theoretically, under this scenario, rich solvent
310 coming out from the absorber bottom should have the same CO_2 loading as that leaving from
311 the bottom of the desorber/reboiler. However, in reality, due to the plant configuration this was
312 not the case. The reboiler is a shell and tube heat exchanger, having solvent on the shell side,
313 which contains most of the solvent inventory, around 90%, of the plant. Rich solvent coming
314 from the absorber mixes with the solvent already in the reboiler and gets diluted so the loading
315 in both the rich and lean is expected to be different depending upon the operational conditions.

316 Rich and lean solvent loadings as measured by Raman probes and titrations are presented in
317 Figure 3. Solid lines are representing continuous measurement by Raman Spectroscopy while
318 point values are representing titration data. Due to the close proximity of manual sampling
319 points and Raman probes, circulation times between them for both the rich and lean solvent
320 streams were less than 5 seconds for all the flow conditions tested. In an ideal situation, for
321 comparison, manual samples should be taken at the exact same time as the Raman sensor
322 updates its output, but it is not possible to time it exactly.

323 As the solvent was used in previous tests, it had some unstripped CO_2 in it so these teste were
324 started with a lean solvent. After starting solvent circulation, samples were taken for titration
325 from both lean and rich solvent streams before the introduction of flue gas. These measurements
326 indicated that, before starting the test, the lean and rich solvent streams had CO_2 loading of
327 0.1419 mol/mol and 0.1534 mol/mol. After starting solvent circulation, synthetic flue gas was
328 introduced to the absorber, causing the rich solvent loading to increase. This highly loaded
329 solvent then mixed with the lean solvent in the reboiler sump. Therefore, lean loading is always
330 lower than the rich loading, also increment in lean loading is more gradual while that in rich
331 loading is relatively sharper, see Figure 3.

332

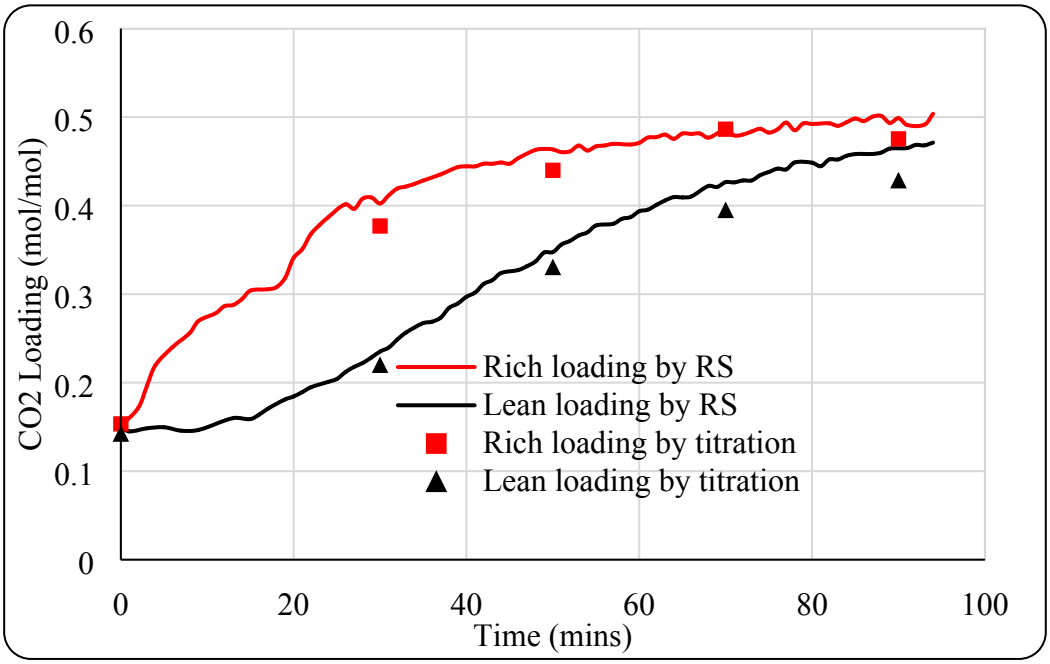

333

Figure 3: Comparison of CO_2 loadings measured by Raman spectrometer and titrations

Figure 3 shows that there is a good agreement between titration data and the Raman predicted values in the whole operation range. During the absorption cycle, the average Raman prediction error was reported as +/-0.009 mol/mol loading by the multivariate model. This concludes that through the Raman prediction curves, it is now possible to discuss and comment on the absorption performance under various process conditions.

As soon as the flue gas was introduced to the absorber, the rich Raman measurement showed an increment in the CO_2 loading while the lean Raman measurement took some time to show the same concentration due to the reasons explained above. Lean loading reached a value of 0.44 mol/mol after around 37 minutes of rich loading. These findings are similar to those demonstrated in Tait et al. (2018) where time to fully mix the contents of the absorber and reboiler for this plant was found to be 37-38 minutes using conductivity probes, one each at the inlet and outlet of the absorber and stripper. This test also proves that the Raman spectroscopy can be used to determine the solvent circulation times inside the plant.

Absorber temperature profile:

Figure 4 plots the temperature profile inside the absorber. The temperatures are plotted against time for different locations along the height of the absorber starting from the bottom of the packing. When flue gas is initially fed to the absorber, temperatures at the bottom of the absorber increased sharply in comparison to those further up in the column. This implies that lean solvent first comes in contact with the flue gas at the bottom. However, after some time, temperatures in the middle of the column increased sharply as compared to those at the bottom and top. Moreover, the temperature bulge is observed at 2/3rd of the packing height, indicating the maximum reaction point. These observations coincide with rich CO_2 loading measurements by Raman Spectroscopy, plotted on the same graph. The Raman predictions of the CO_2 loading in the rich amine stream is increased drastically until the temperature profile inside the absorber reaches its maximum. The temperatures started to decrease as the gradient of the increment in CO_2 loading in the rich amine stream was decreased. This is due to the temperature dependency and exothermic nature of the CO_2 absorption process. As the difference between the lean and rich loading is decreased, proportionally the temperatures inside the absorber also drop. This absorption test confirms that both Raman probes measurements in lean and rich streams were able to follow the absorption phenomenon.

Capture efficiency:

Concentration of CO_2 in the inlet gas was fixed at 12%. Concentration of CO_2 in absorber exit gas increased gradually from below 1% to close to 12%. Figure 5 plots CO_2 capture efficiency against time during the absorption process. As can be witnessed from the plot, at the start of the test, capture efficiency was around 97% and it remained almost steady for about 14 minutes, at which point it dropped sharply and steadily to below 20% within one hour. As solvent was not being stripped, its loading capacity gradually reduced and reached a point where there was no further absorption i.e. concentration of CO_2 in the gas leaving the absorber was approximately the same as that entering the absorber.

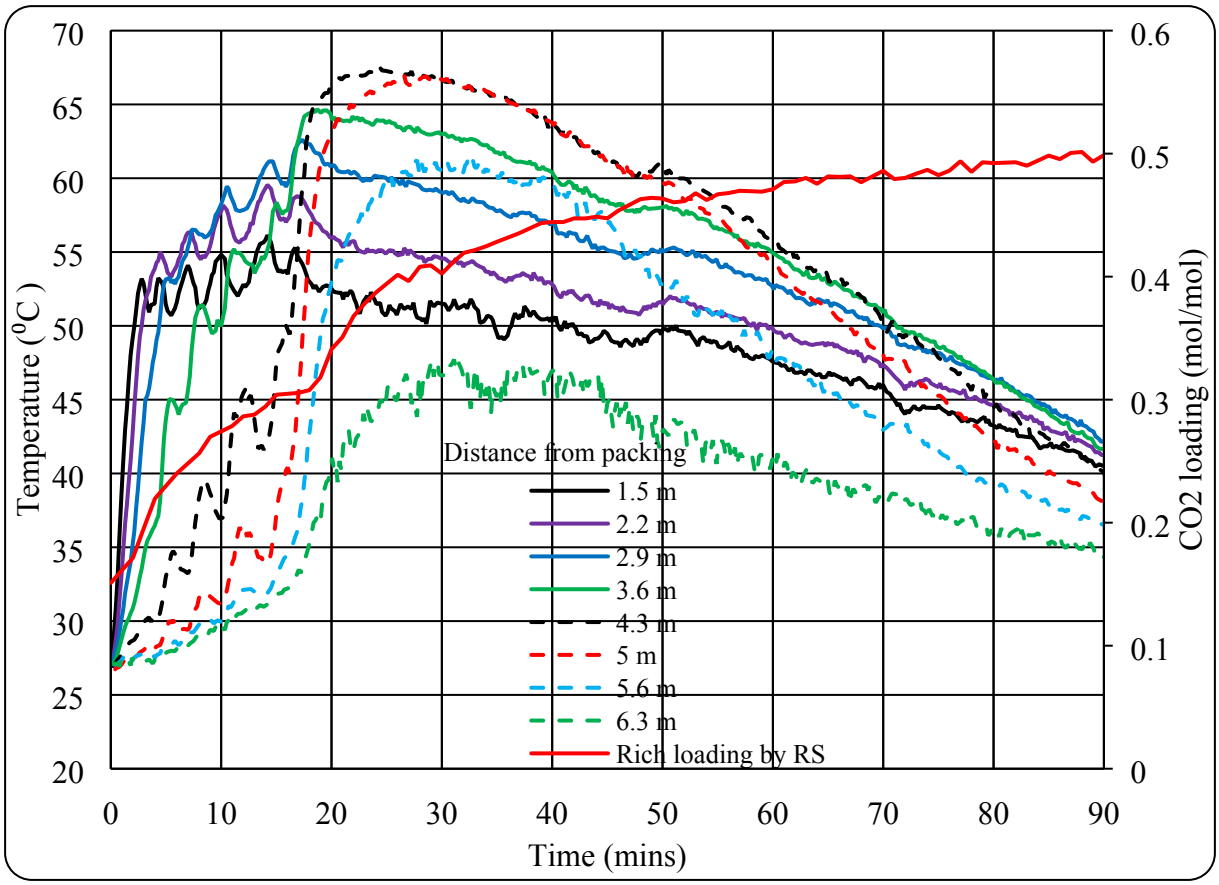

Figure 4: Absorber temperature profile during absorption cycle (Temperature measurements locations are measured from the bottom of packing)

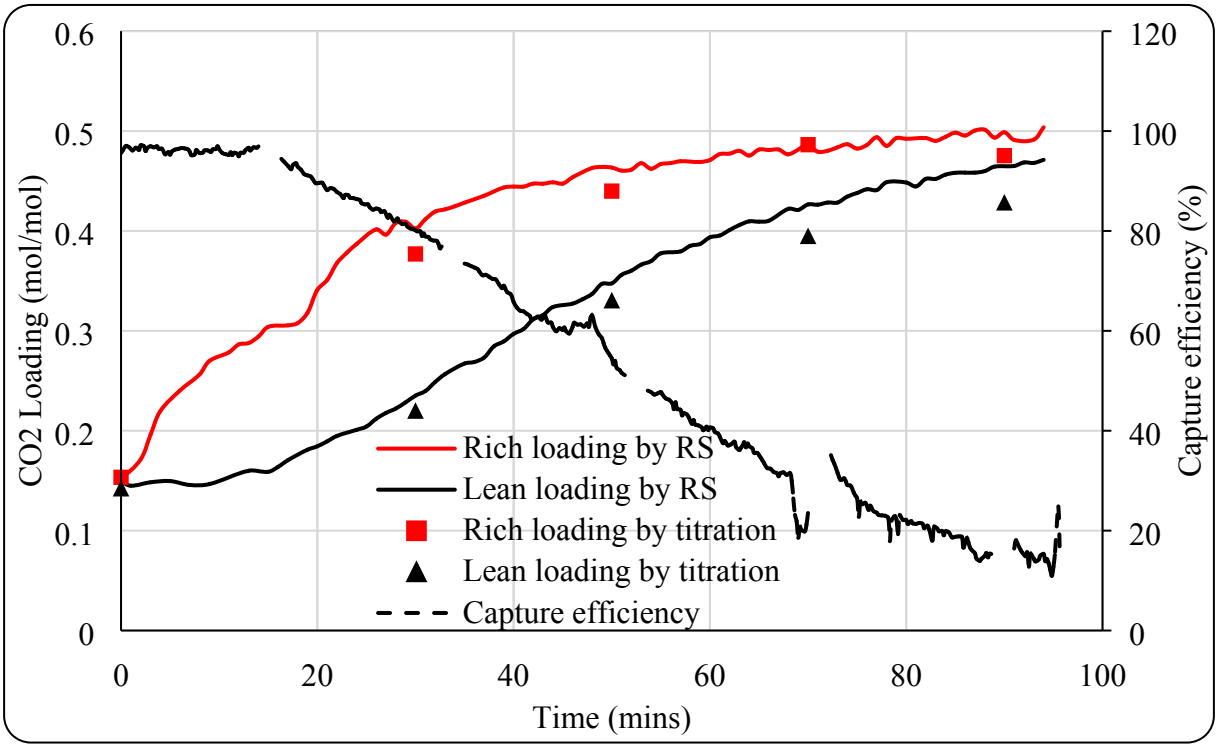

Figure 5: Capture efficiency change with time during absorption

The Raman measurements plotted on the same graph also show the same trends. At the beginning both of the loadings were almost the same. Then, rich loading started to increase sharply as flue gas was introduced. Lean loadings started to increase with some delay caused by the solvent inventory in the reboiler sump. Raman measurements indicate that difference between rich and lean loadings was quite high for around 45mins of the test period and then started dropping as capture efficiency reached below 55%. Towards the end of the absorption test, both of the loadings again become closer to each other towards the rich loading limit of the solvent.

As CO_2 injection rate is controlled separately and is not directly linked to concentration of CO_2 in the flue gas, at around 70 minutes, CO_2 concentration dropped to 11% due to some process issues. Due to this reason the capture efficiency plot shows an increase at this time.

Emissions:

Figure 6 shows emissions of MEA and ammonia during the absorption process. MEA emissions were observed to be very high at the start, then reduced to almost zero after 13 minutes and remained low throughout the test. The initial high level of MEA was thought to be due to the start of the process. At the start solvent is very lean and reaction rate between MEA and CO_2 is relatively higher. Higher rate of reaction can result in higher rate of degradation and thus can be the cause of higher MEA evaporation from the absorber. However, most of the MEA carried over with the flue gas from the absorber was removed by water wash. The FTIR instrument is installed on upright pipe so there is a U-bend just before the measurement. The carried over water and solvent from the absorber tend to condensate and accumulate in the U-bend. A drain is provided at this point which feeds condensate back to the absorber. However, sometimes the U-bend does not drain fully and result in flash of the condensate into the sampling point filter resulting in increased MEA point measurements. The occasional peaks of 20-30 ppm of MEA observed in Figure 7 are due to this phenomenon.

Degradation of MEA during the cyclic operation is a significant problem. Knudsen et al. have reported a loss of MEA of 2.4 kg per ton of CO_2 captured [Knudsen et al. 2007]. The degradation can happen by two mechanisms. Thermal degradation occurs at stripper conditions, high temperature and abundance of CO_2 [Rochelle, 2012, Kohl and Nielsen, 1997]. Oxidative degradation occurs at lower temperature and in the presence of oxygen. These conditions are available in the absorber. It is thought that oxidative degradation is dominant degradation pathway for MEA [Da Silva et al. 2012, Lepaumier et al. 2011]. Leonard et al. [26] proposed a model for oxidative degradation described the following over all reaction.

$$MEA + 1.3\ O_2 \rightarrow 0.6\ NH_3 + 0.1\ HEI + 0.1\ HEPO + 0.1\ HCOOH + 0.8\ CO_2 + 1.5\ H_2O$$

The reaction indicates that Ammonia is the main degradation product which exits with the flue gas. It is essential to monitor the emissions of ammonia during the process to assess environmental burden of the process. Ammonia emissions started at a value of around 30ppm and peaked at 67ppm. After this the emissions started decreasing and become very low to a value of below 10ppm. The emissions seem to follow the absorption phenomenon as can be observed from rich and lean loadings as measured by Raman probes. Ammonia emissions increase at the start due to increase in loading due to absorption of CO_2, reaches a peak value and then start decreasing due to drop in reaction rate. The similar phenomenon is followed by

Raman measurements indicating that Raman Spectroscopy can be employed to monitor process variations in CO_2 capture plants.

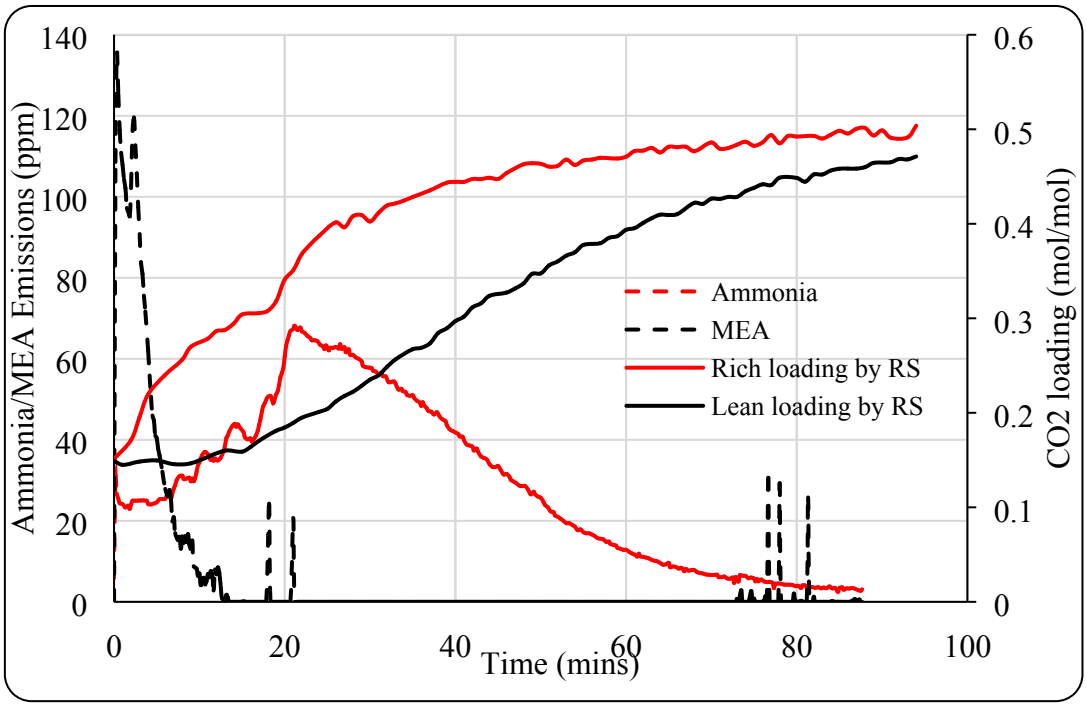

Figure 6: Emissions of MEA and Ammonia (NH_3) during absorption process

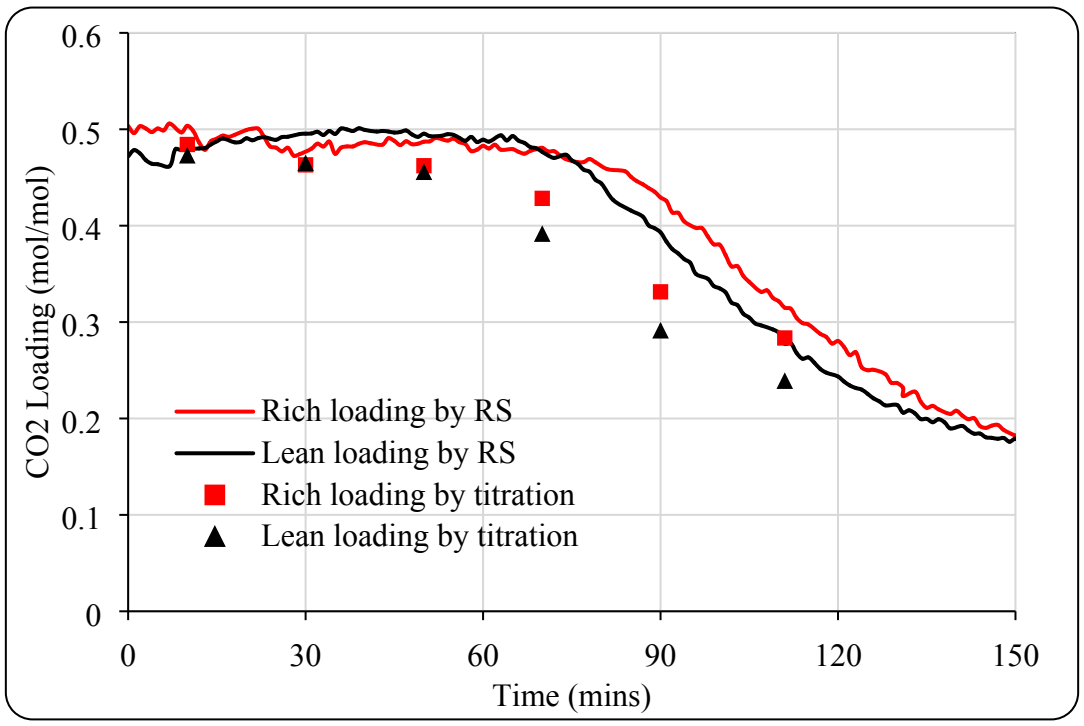

Figure 7: Comparison of CO_2 loadings during desorption measured by Raman spectrometer and titrations

3.2.2. Desorption

After completion of the absorption cycle, flue gas was turned off and desorption cycle was started by supplying pressurized hot water to the reboiler. The aim of this desorption cycle test is to monitor the predictive capacity of Raman instrument during a complete desorption cycle in which CO_2 is stripped from saturated solvent. Figure 7 shows the comparison of Raman predictions in rich and lean solvent streams with respect to the titration measurements. Both rich and lean loadings start dropping after some time of starting the desorption cycle. The delay was due to the time taken for the solvent to heat up. Both of the loadings drop due to CO_2 being stripped from the solvent but no absorption due to stoppage of flue gas to the absorber. Both the rich and lean Raman measurements are high than the titration data. This may be due to the same model being used to predict both of the data sets.

Similar to the absorption cycle, during the entire desorption phase, the inline Raman predictions show good agreement with the offline measurements by conventional titration methods. However, during desorption cycle rich and lean loadings are closer to each other as compared to absorption cycle. This is due to less solvent inventory in the absorber, only 10% of the total plant inventory. Lean solvent from desorber mixes with the solvent in the absorber sump and thus loading changes.

Temperature distribution in the stripper:

The stripper temperature profile is plotted against time alongside CO_2 loading measurements by Raman probes, in Figure 8. The Fig shows that temperatures throughout the stripper column are identical throughout the test. The temperatures increase linearly at the start of the PHW supply until reaching a peak value before becoming steady. Total time for stripping was calculated to be 3:20 hrs. The figure also shows that Raman measurements follow the desorption process. Plot indicates that both rich and lean Raman measurements became closer after stopping absorption due to continued circulation as stripping was not started for a while even after PHW flow was started. Both the rich and lean loadings started dropping as the solvent heated up to the stripping temperature. The stripping rate was very high as column temperatures increase above 80 ^{0}C. This is marked by a rapid drop in both rich and lean loadings for around 1.5 hrs, after which the stripping rate dropped and loadings did not change as much. Both of the Raman probes followed the same trend with rich probe measurements are little higher than the lean ones due to mixing with rich solvent in the absorber sump. The stripping process was stopped by ceasing PHW supply to the reboiler when Raman measurements dropped to around 0.15 as it is not worth striping to lower loadings as it can result in dramatic increase in reboiler duty.

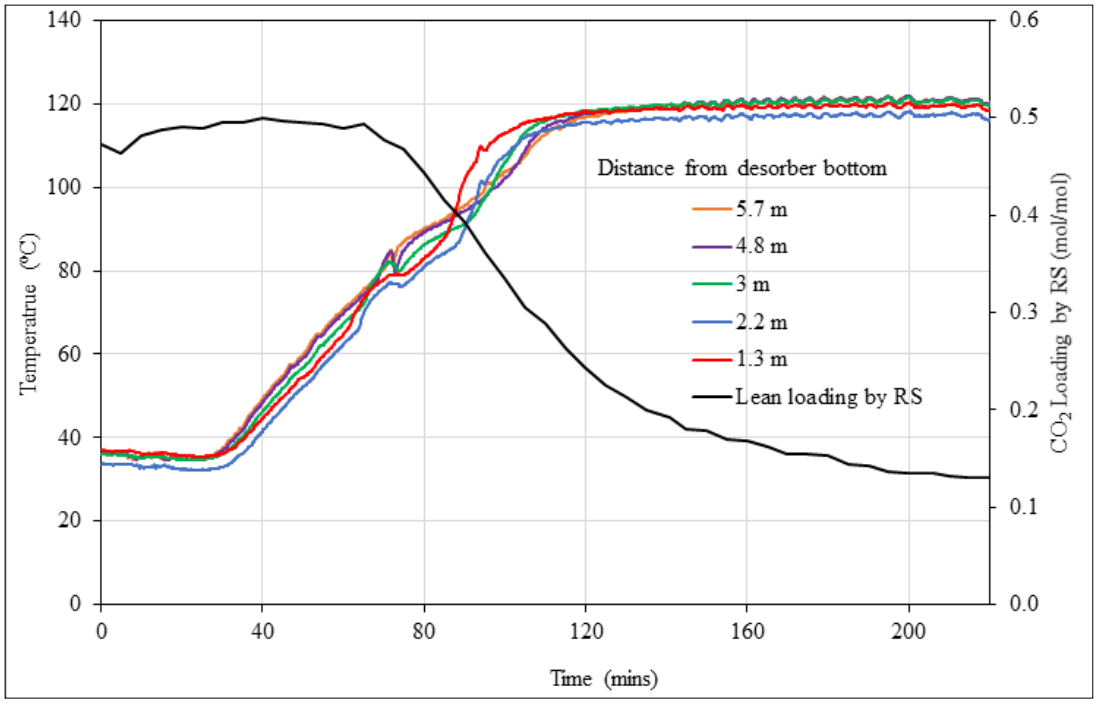

Figure 8: Stripper temperature profile during desorption process

Emissions:

During the desorption cycle the stripper outlet CO_2 stream was monitored via FTIR analyzer. Concentration of MEA in the CO_2 stream is plotted against time in Figure 9. After 43 mins of opening the pressure control valve MEA emissions reached a peak value of 55 ppm and then started dropping.

Similar phenomenon was observed during absorption, where MEA emissions were higher at the start, then dropped as the process progressed indicating that solvent emissions are higher at the start of the process and then decrease as the process moves towards steady state. In the case of desorption, pressure control valve stays closed until pressure is built up to the set point. In Figure 9 for example the valve started opening at 65 mins. Up to this point any condensation of MEA is accumulated behind the control valve. The accumulated MEA leaves with the product gas when the pressure control valve opens. This is the reason the MEA emissions increased first then dropped to around 10 ppm. A steady test on this plant usually takes around 3-5 hrs depending upon the parametric changes. MEA emissions with the product gas during this period under the test conditions are estimated to be around 2 g.

Raman measurements for lean loading are also plotted in Fig 9. The plot indicates that MEA emissions start to increase as stripping process started as indicated by drop in loadings measured by Raman probes. Emissions started to drop as stripping process became slower and loadings dropped to lower values.

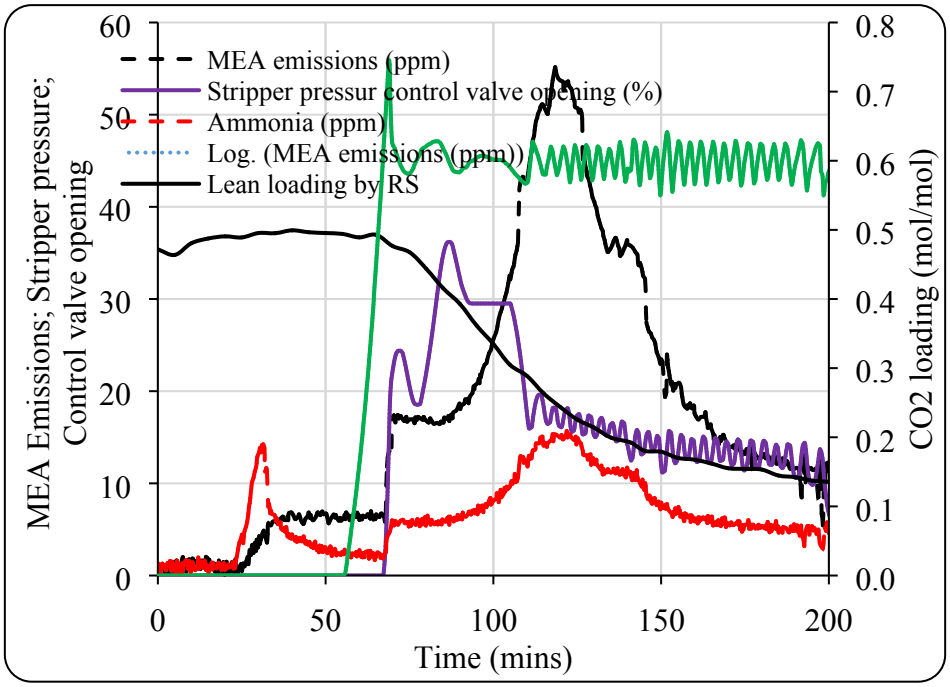

Figure 9: MEA emissions during stripping process

3.3 Tests with process conditions variations

During these tests, process conditions were varied. The test was started with 600 kg/h solvent flow and 193 m^3/h gas flow with 5% CO_2 concentration (Test 3). The process parameters varied during the trial were increase/decrease in flue gas flowrate, CO_2 content (%vol) of the flue gas and solvent flow rate. Figure 10 shows the comparison of the rich and lean Raman measurements with the manual titration values. The rich and lean loadings first increase and then decrease without any process changes. This is due the fact that when the flue gas feed is started, solvent is lean. After the flue gas start up solvent starts absorbing CO_2, loadings start to increase but after some time when the solvent in the stripper is hot enough for stripping, the loadings start to drop.

The rich loading reached a maximum value of 0.44 mol/mol after CO_2 concentration was changed from 5% to 12%, (Test 4) while the lean loading remained between 0.108 mol/mol and 0.229mol/mol during the entire test campaign. The figure shows that rich Raman measurements have better fit with the titration data as compared to lean Raman measurements.

The impact of step changes in these parameters is more significant on the rich loading than that on the lean loading. The impact of process variations on the lean loading is delayed and dampened by dilution and mixing effects due to high solvent inventory in the reboiler. Therefore, it takes some time for the process changes effecting the rich solvent to be reflected in the lean solvent.

In the lean stream, the deviation of Raman measurements with respect to the titration results is higher as compared to that in the rich stream. This could be, due to the noise from new immersion probe and the new fibre optic cable connected to the lean stream. The multivariate model used in this study was developed from calibration and validation using the same immersion optic probe and fibre optic cable which were connected to the rich stream. Therefore, the instrument related noise from rich measurements are already accounted for in

the calibration model, whereas those from lean measurements are not encompassed. The deviation between the lean Raman measurements and lean titration values can be reduced by updating the existing calibration model by including new calibration samples from this PACT test campaign (Jinadasa, 2019).

Figure 11 plots process variations alongside loadings data. The plot shows changes in CO_2 loadings as measured by Raman probes with respect to change in CO_2 concentration in the flue gas. As the CO_2 concentration was changed from 5 to 12%, rich loading increased rapidly from around 0.26 to 0.44 mol/mol. Lean loading increased steadily following a delay due to circulation times and mixing in the reboiler tank.

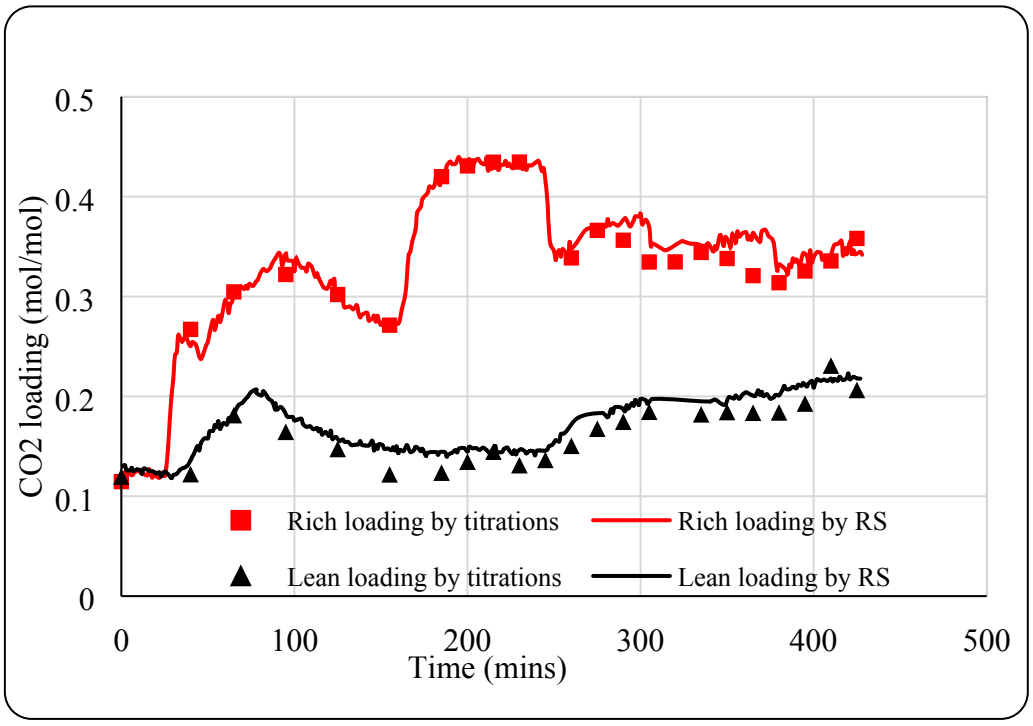

Figure 10: Comparison of Raman measurements and titration results for process variations

Figure 11 also plots solvent flow rate variations alongside Raman measurements against time. The tests were started at 600kg/h solvent flow rate, which was changed to 1000 kg/h and 1200 kg/h during the course of the tests. As the solvent flow was increased from 600 to 1000 kg/h, Raman probe shown a sharp drop in rich loading, from 0.42 mol/mol to 0.33 mol/mol, then started increasing slowly. Lean loading measured by lean Raman probe also shown a slight drop and then started increasing slowly, lean amine loading increased from 0.148 to 0.179 mol/mol as the solvent flow rate was increased. As a result of increase in solvent flow rate, residence time in the reboiler decreased, resulting in drop in degree of stripping as the PHW supply conditions to the stripper remained the same. Due to increase in lean loading, rich loading also started increasing as absorber was receiving solvent with relatively higher lean loading.

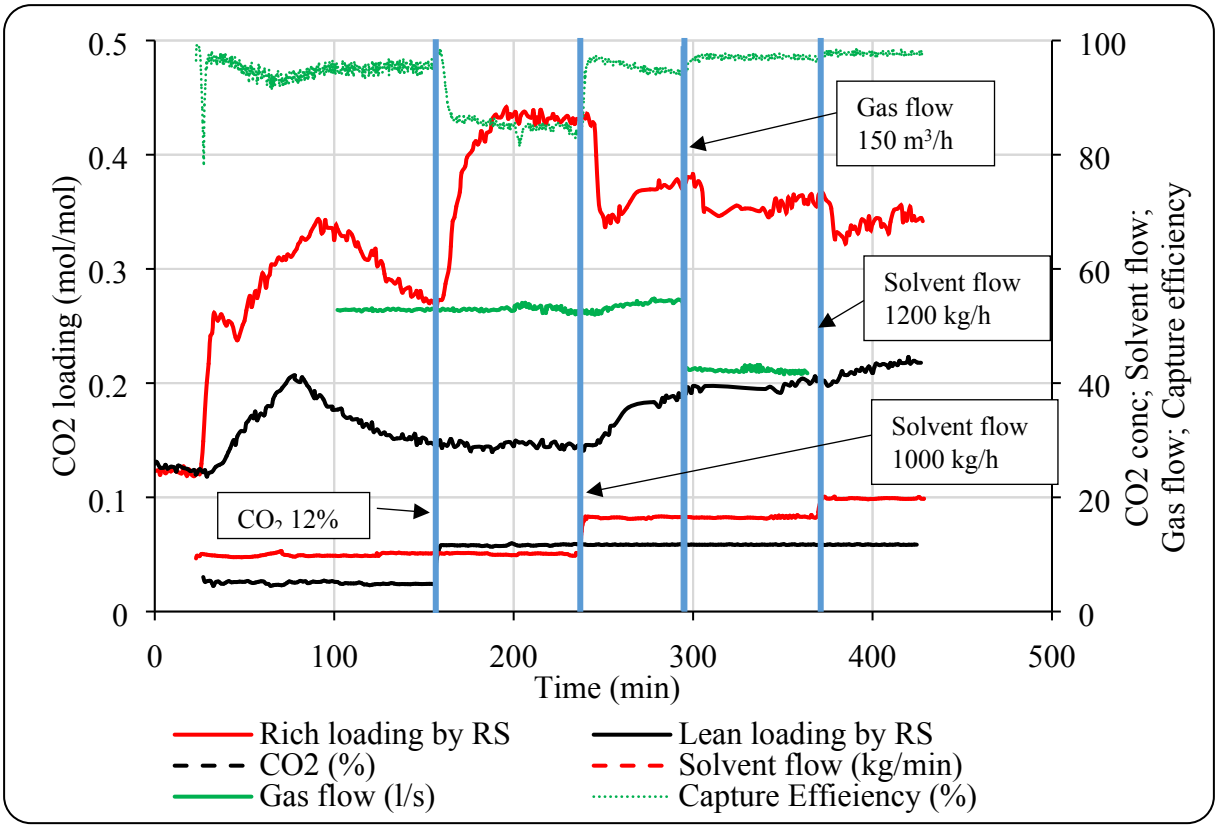

Figure 11: Change in rich and lean loading with parametric variations

A similar phenomenon was observed when solvent flow rate was further increased to 1200kg/h. The rich Raman probe shown a drop in rich loading while lean Raman probe indicated a gradual increase in lean loading.

Figure 11 also plots variation in flue gas flow rate alongside Raman measurements against time. When flue gas flow rate was dropped from 190 m^3/h to 150 m^3/h, drop in rich loading was recorded by rich Raman probe. Lean Raman probe also shown a drop in lean loading at this point because solvent entering into the stripper was less loaded and due to stripper conditions unchanged, solvent leaving the stripper was also less loaded, although not proportionately.

Results indicate that even though there were several different process changes happening over a relatively short period of time, the Raman prediction model managed to observe the small changes in solvent loading and agreed well with titration results.

Capture efficiency:

Capture efficiency is also plotted, against time, in Figure 11 alongside rich loading as measured by Raman probe. It can be seen from the plot that the capture efficiency was relatively higher, averaging around 95%, when 5% CO_2 concentration flue gas fed into the absorber. When the CO_2 concentration was increased to 12%, capture efficiency dropped to around 85%. During this test rich Raman measurements recorded a considerable increase while capture efficiency dropped indicating that the solvent did not have much capacity left in it to absorb a step in change in CO_2 concentration from 5% to 12%. Therefore, solvent flow was increased in the following test to increase solvent capacity. In this case, capture efficiency increased back to above 95% and rich loading dropped. Similar phenomenon can be observed for tests 6 and 7, where flue gas flow was decreased to 150 m^3/h and solvent flow rate was increased to 1200

kg/h, respectively. In both cases capture efficiency increased but rich loading decreased due to increase in solvent capacity as result of increase in L/G ratio.

Absorber temperature profile:

Absorber temperature profile is plotted against time along the absorber height form the bottom of the packing alongside Raman measurements in Figure 12. The temperature profiles at different times indicate the effect of changes in operational parameters on the profile. It can also be noted that the temperature profiles vary proportionally to the Raman measurements for rich CO_2 loadings. The location of the peak (bulge) temperature in the absorber, varied with variations in process parameters.

At low CO_2 concentration of 5% v/v (Test 3), the highest temperature (57 ^{0}C) was recorded just above the middle of the column, between 3.6m and 4.3m from the bottom of the packing. The top temperature measurement shown the lowest reading during this test due to most of the reaction happening in lower part of the column and relatively cold lean solvent entering from the top.

As the CO_2 concentration was increased from 5% to 12% (Test 4), bottom two temperature measurements recorded a drop in temperature while rest of the six measurements recorded an increase. The bulge temperature increased by 11 ^{0}C to 68 ^{0}C as the concentration was increased to 12%. However, temperature at the bottom (1.5m) of the column dropped. Capture efficiency dropped from above 95% for Test 3 to around 85% for this test due to the reason that solvent flow rate is too low to absorb any more CO_2.

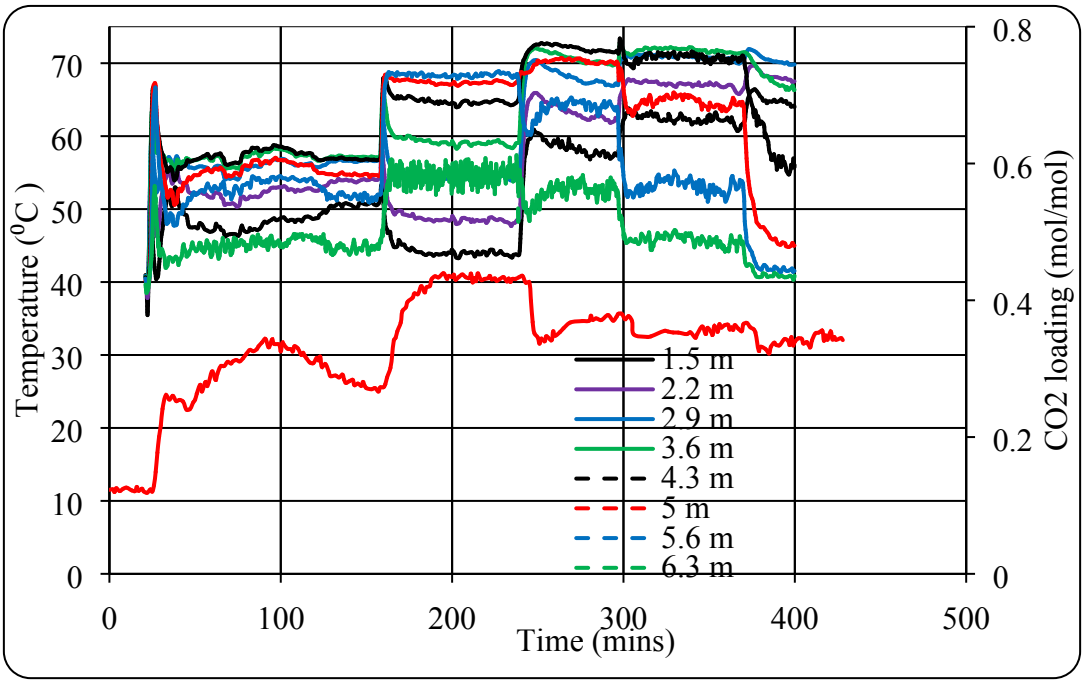

Figure 12: Changes in absorber temperature profile and Raman measurements with variations in operational parameter

It can be witnessed from the plot that rich Raman probe recorded a sharp increase in rich loading at this point which indicated that the Raman measurements followed the process. The bulge

590 also shifted up in the column, between 5m and 5.6m, as the CO_2 concentration was increased
591 to 12%. However, in this case the lowest temperature was recorded at the bottom of the column
592 rather than at the top as in the case of 5% CO_2. This is because most of the reaction happened
593 towards the top of the column and incoming lean solvent was heated by the outgoing, relatively
594 hot gas.

595 The poor performance of the absorber in this test could be due to the combination of the
596 following two reasons.

597 1. Solvent flow of 600 kg/h is too low for the absorption of CO_2 from the flue gas under
598 these operational and absorber design conditions.
599 2. The top of the absorber has pinched performance i.e. there is virtually no driving force
600 for absorbing any more CO_2. The phenomenon is referred to as chemical equilibrium
601 pinching [Brigman et al. 2014] i.e. if lean loading is not sufficiently low (solvent does
602 not have sufficient capacity), CO_2 equilibrium partial pressure in the lean stream
603 entering the absorber is close to the partial pressure of CO_2 in the gas leaving at the top
604 of the absorber. Under these conditions, mass transfer will drop in the upper section due
605 to lower mass transfer driving force available. In order to avoid such a situation, lean
606 loading should be dropped by increasing stripper temperature.

607 The bulge temperature further increased to 73 ^{0}C as the solvent flow rate increased to 1000kg/h
608 (Test 5) indicating an increase in absorption rate. However, the location of the bulge
609 temperature shifted downwards to 4.3m location. Again, the lowest temperature was recorded
610 at the top of the column due to shift of the reaction towards the lower part of the column. This
611 argument is also justified by around 15 ^{0}C increase in temperature at the bottom of the column
612 due to relatively hot solvent flowing down to the lower section of the column.

613 The bulge temperature stayed almost the same at 73 ^{0}C when flue gas flow rate was dropped to
614 150 m^3/h (Test 6). It is interesting to note here that the cold part at the top of the column
615 elongated and second last temperature probe (5.6m) also measured temperature lower than the
616 bottom of the column. The bottom temperature further increased to close to the one measured
617 at 5.3m. Another interesting phenomenon noted here is that bottom 6 measurements are closer
618 as was the case in Test 3 while Tests 4 and 5 shown wider scattered temperature distribution.

619 As the solvent flow rate was increased to 1200 kg/h (Test 7), absorber temperatures shown an
620 interesting phenomenon. Bottom three temperatures shown an increase while rest of them
621 shown a drop. It is interesting that bottom four measurements recoded higher temperatures than
622 the top four. For the first time the bulge temperature recorded was in the lower half section of
623 the packing, at 2.9m, indicating that the reaction was shifted towards the lower section of the
624 column due to high liquid to gas ratio. Test 7 temperature profile indicates that the column is
625 pinched at the bottom, rich end. The rich end pinch occurs due to mass transfer limitations and
626 is independent of bulge temperature (Sachde *et al.*, 2014).

627 These observations indicate that absorber temperature profile is dependent on operational
628 conditions and that the bulge temperate shifts as the operational conditions are varied. So,
629 determination of the optimum location for solvent intercooling will be different for different
630 flue gas compositions, operational conditions and plant configurations and must be determined
631 on case by case basis. Moreover, the findings suggest that Raman Spectroscopy has the

capability to follow variations in process and can be employed for real time monitoring and control of the CO_2 capture process.

Emissions:

Emissions of MEA and Ammonia as measured by FTIR at the outlet of the absorber are plotted in Figure 13. The figure indicates that emissions are higher at higher L/G ratio (Tests 5-7) as compared to those at low L/G ratio (Tests 3&4). Emissions of MEA were around 40 ppm during low L/G ratio tests, but peaked to above 100 ppm for the higher L/G ratios. However, the water wash has shown to remove most of the solvent from the gas before exiting to atmosphere. Emissions of Ammonia, after initial peak at the startup, dropped to around 5ppm and stayed low for low L/G ratios but started increasing as L/G gone up.

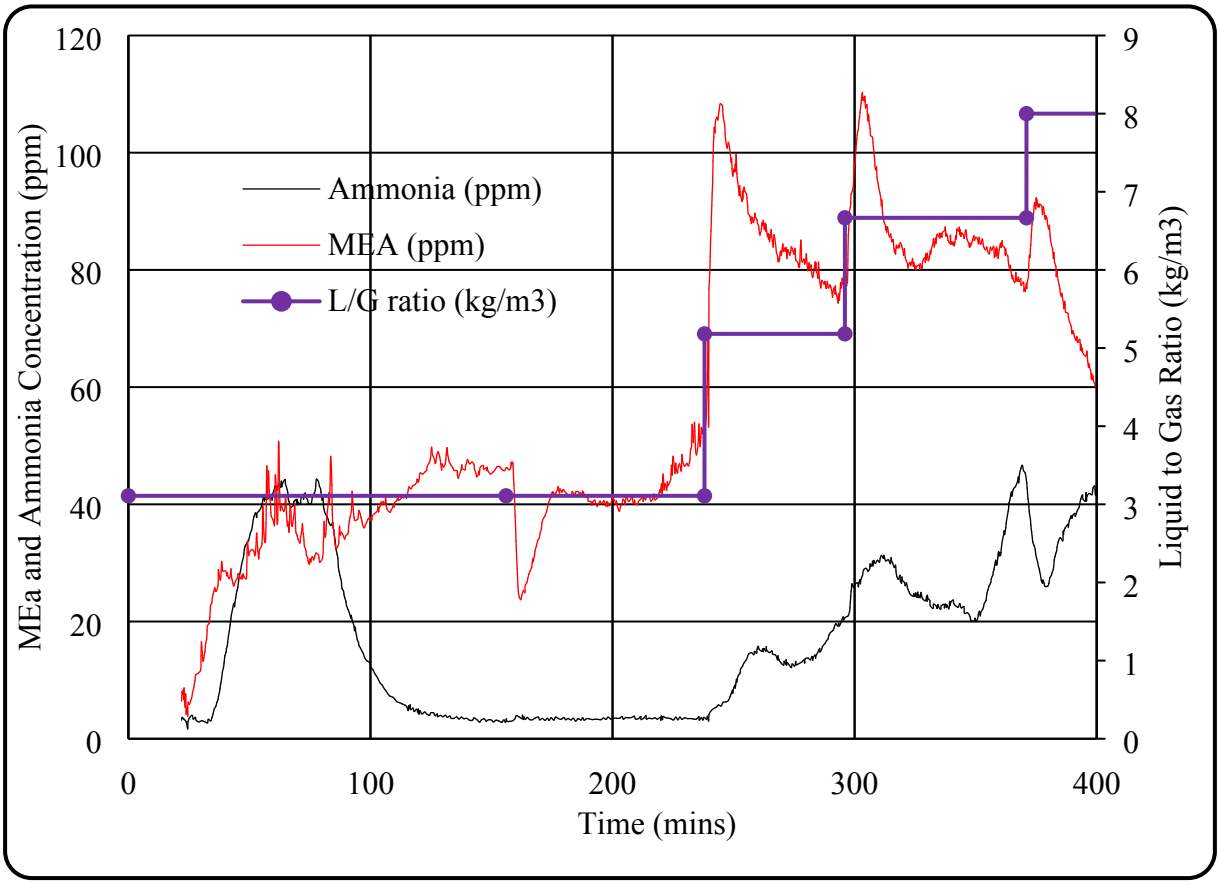

Figure 13: Emissions at the outlet of the absorber for process variation tests

3.4 Coal Flue gas (with Sulphur dioxide)

For these tests, flue gas from a coal firing pulverized fuel combustor, containing 210 ppm of SO_2 on average, was fed to the capture plant. The aim was to investigate if Raman measurements are affected by solvent degradation. Operational condition for this test are given in Table 4. Similarly to the previous cases, manual samples were taken from the plant and titrated for CO_2 loadings and MEA concentration. Figure 14 compares Raman predictions with

titration results for rich and lean loadings. The real time Raman predictions and the offline titration results show a satisfactory agreement throughout the entire process.

Rich loading drops sharply just after 200 mins of operation, see Figure 14, at this point the plant was tripped and flue gas flow was ceased. The effect of plant trip is shown by drop in lean loading after some time due to the reasons explained previously in this paper.

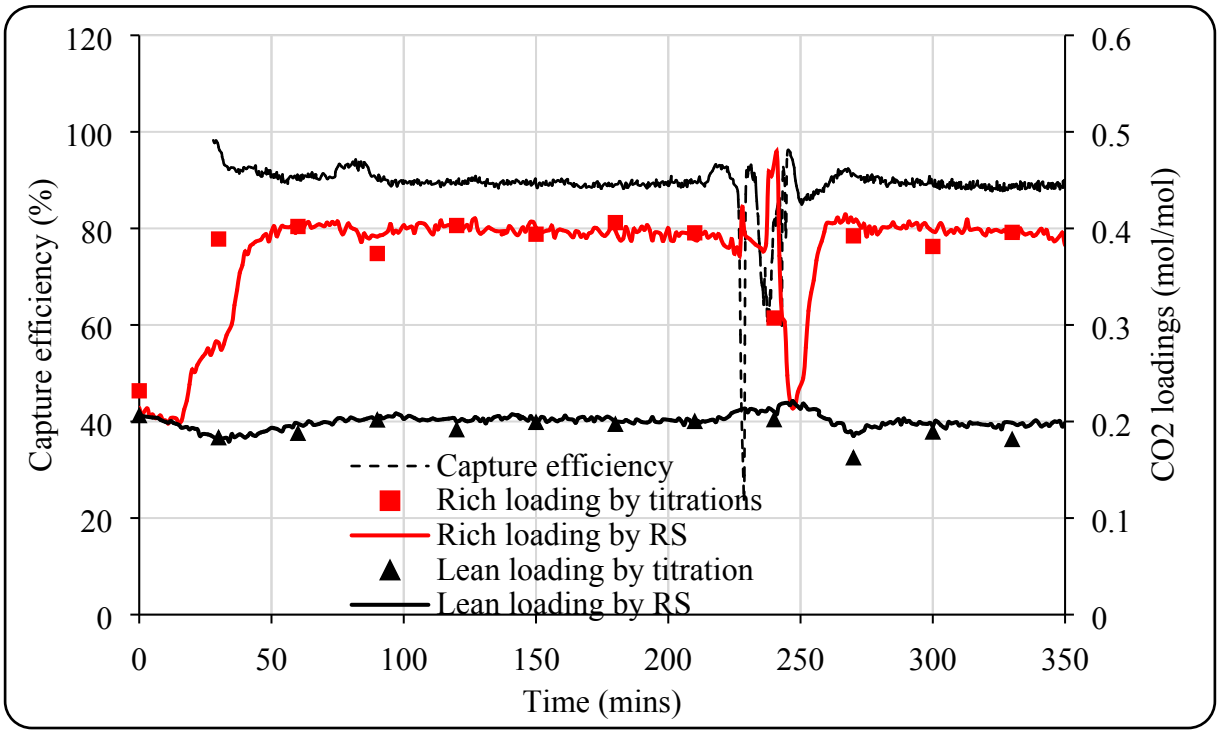

Figure 14: Comparison of rich and lean Raman measurements with titration data

The close agreement of Raman measurements with titration data provide evidence for the accuracy of Raman predictions with respect to titration results. It can be concluded that the presence or absence of SO_2 in the flue gas has not affected the CO_2 loading predictivity by the Raman models which were developed based on partial least squares (PLS) algorithm.

Capture efficiency:

Figure 14 also plots capture efficiency as a function of time for tests with coal flue gas. The plot shows that the capture efficiency was maintained around 90% throughout the test, except when the plant has start/stop due to tripping. The same phenomenon is observed with rich and lean Raman measurements, also plotted in Figure 14, where both the rich and lean loadings are more or less unchanged.

Temperature profile:

Figure 15 shows absorber temperature profile for test with coal flue gas. It can be observed from the plot that the highest temperature was measured at about 1/4th of the packing from the top. The plot is showing temperature dips at around 2/3rd of the test period. As mentioned previously, plant tripped at this point and all the flows stopped but was restarted promptly.

A close look at the temperature profile reveals that the temperature profile is different before and after the plant has tripped. The reason for that is the change in temperature of lean solvent

entering the absorber. The temperature of the leans solvent was controlled at 40 ^{0}C and 50 ^{0}C, before and after the plant trip, respectively. In both the cases, the temperature bulge is at almost the same location but bulge temperature is little bit higher in the case of 50 ^{0}C. Moreover, temperatures in the top half of the column are generally higher in the case of 50 ^{0}C lean solvent temperature while those at the bottom of the column are not changed much.

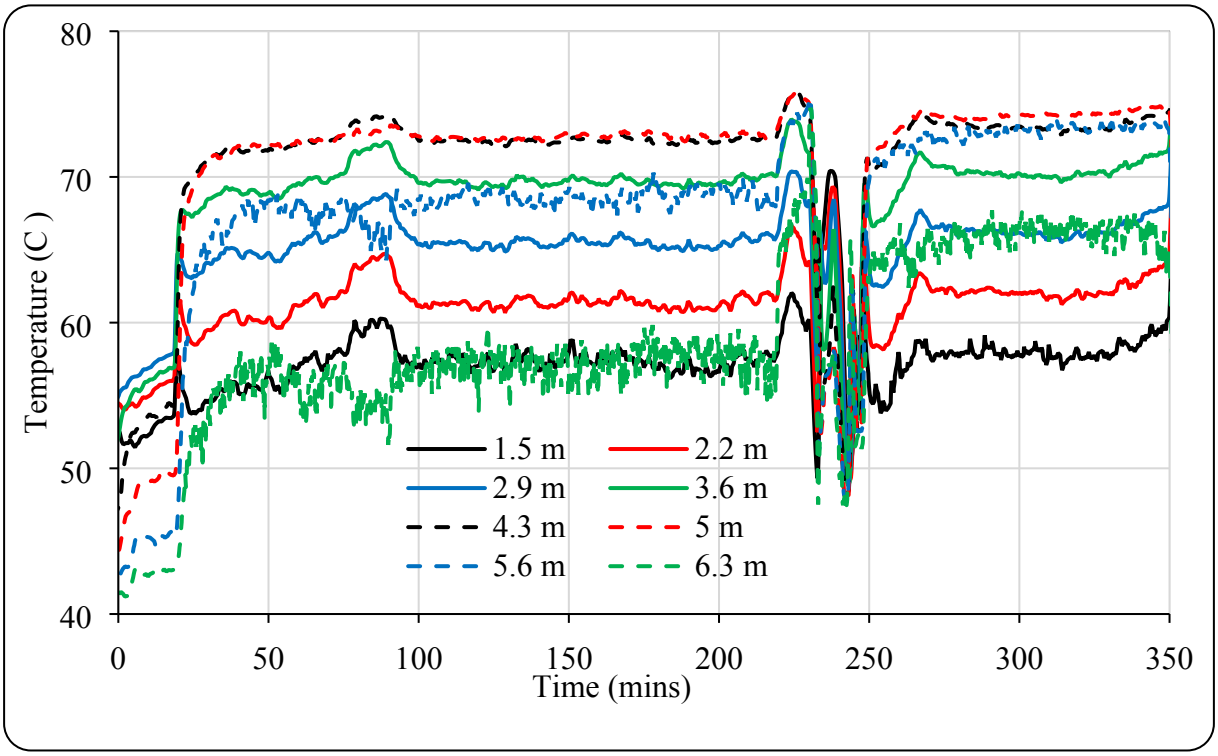

Figure 15: Absorber temperature profile for coal flue gas – temperature locations are from bottom of the packing

Emissions:

Figure 16 plots emissions of ammonia and MEA at the exit of absorber for the coal flue gas tests. It can be observed from the plot that emissions increased with time. This is due to the persistent supply of 210 ppm of SO_2 in the flue gas resulting in degradation of solvent. The continuous increasing trend in emissions indicate that solvent degradation rate was increasing. The close agreement of Raman measurements with the offline titrations, even during accelerated degradation, indicates that the Raman model developed here can be used to monitor the capture plant performance.

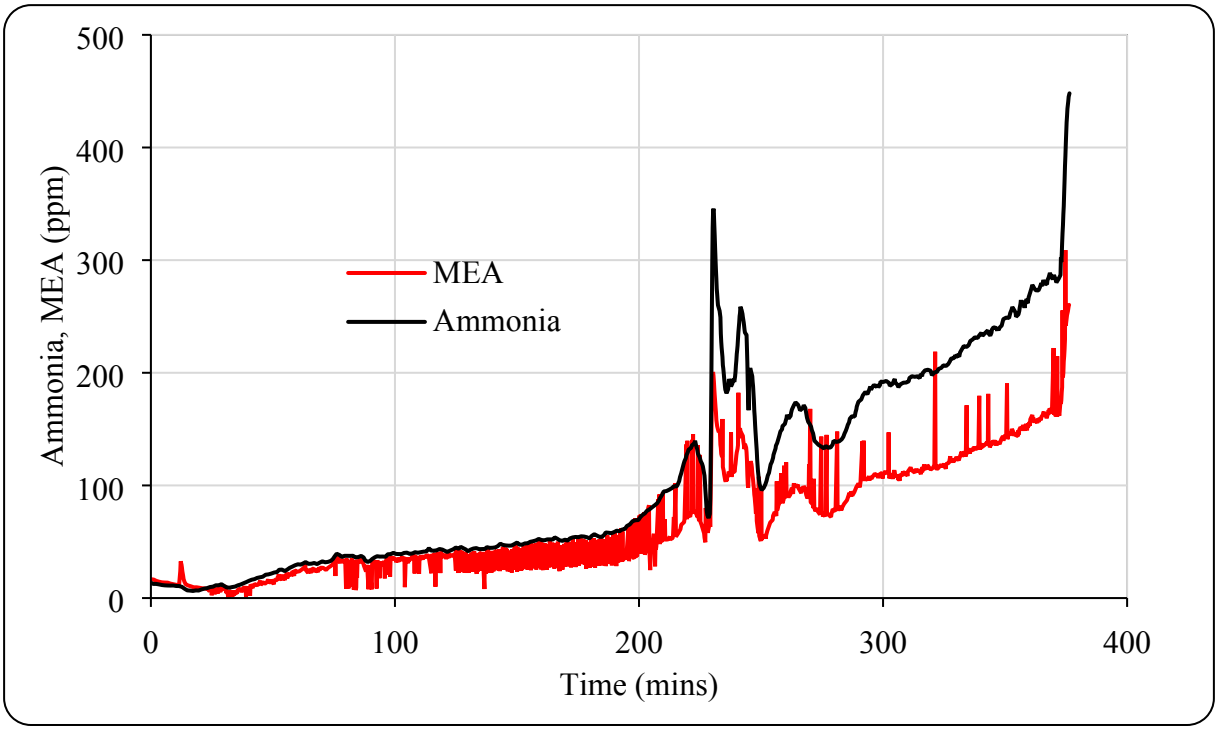

Figure 16: Emissions during coal flue gas testing

4. Conclusions:

Solvent monitoring is very critical particularly in the case of dynamic CCS plant operation. Manual sampling is a labor-intensive task and has health and safety implications, including access to sampling points, harsh process conditions and chemical exposure. Moreover, it takes time to process samples and thus sampling frequency is reduced resulting in potentially loosing critical data variations in the plant operation. There are several and complex mathematical and thermodynamic modeling developed to understand the CO_2 capture plant performance with respect to different process conditions in literature. Most of these models are limited to pen-and-paper due to the lack of validation with test results.

The Raman spectroscopic real time monitoring tool developed here is validated against pilot plant data in stable and dynamic conditions in both the absorption and desorption processes of CO_2 capture plant. Such a tool is one of most-awaited requirement in a CO_2 capture plant and its journey towards commercial deployment. The application of such a tool to the real time monitoring of capture plant can reduce the plant downtime, time and resources spending on offline analysis and provide the plant operator a better overview about the past-present plant conditions and ease to take decisions to optimize the plant operation. As Raman predictions can provide reliable real time measurements of rich and lean CO_2 loading at one-minute intervals, the validation of this analysis is apparent. Based on the tests carried out during these campaigns, following conclusions can be derived.

- Reliability of the Raman predictions are confirmed with the titration measurements carried out in this trial. Raman predictions can be mapped with the changes of process conditions and their intensities. They also provide information on stability of the plant.
- The Raman predictions models are not affected, with accelerated solvent degradation and increased emissions, during 180-235 ppm of SO_2 supply in the flue gas.

The test campaign at the PACT CO_2 capture plant with real time solvent monitoring using Raman Spectroscopy has demonstrated that the technology is a step closer to making offline measurements a thing of the past and moving towards predictive control of CO_2 capture plants.

5. Acknowledgement:

The authors would like to acknowledge the financial support of the UK Carbon Capture and Storage Research Centre and PhD scholarship funded by University of South-Eastern Norway for carrying out this research work. The authors also acknowledge that the PACT Facilities (https://pact.group.shef.ac.uk), funded by the Department for Business, Energy and Industrial Strategy and the EPSRC, have been used for the research work reported in this publication.

6. References:

Abu-Zahra, M.R.M., Schneiders L.H.J., Niederer J.P.M., Feron P.H.M., Versteeg G.F., (2007). CO_2 capture from power plants: Part I. A parametric study of the technical performance based on monoethanolamine, International Journal of Greenhouse Gas Control, Volume 1, Issue 1, April 2007, Pages 37-46.

Ahn, H., Luberti, M., Liu, Z., Brandani, S., (2013). Process configuration studies of the amine capture process for coal-fired power plants. Int. J. Greenh. Gas Control 16: 29–40.

Akram M., Ali U., Best T., Blakey S., Finney, K.N., Pourkashanian M., (2016). Performance evaluation of PACT Pilot-plant for CO_2 capture from gas turbines with Exhaust Gas Recycle, International Journal of Greenhouse Gas Control, Volume 47, April 2016, Pages 137-150.

Amrollahi, Z., Ertesvag, I.S., Bolland, A., (2011). Optimized process configurations of post-combustion CO_2 capture for natural-gas-fired power plant-exergy analysis. Int. J. Greenh. Gas Control 5: 1393–1405.

Andersson, V., Wittmeyer, K., Gorset, O., Maree, Y., & Sanden, K. (2013). Operational Experience and Initial Results from the First Test Period at CO_2 Technology Centre Mongstad. Energy Procedia, 37, 6348-6356. https://doi.org/10.1016/j.egypro.2013.06.564

Aronu, U.E., Svendsen H.F., and Hoff, K.A., (2010). Investigation of amine amino acid salts for carbon dioxide absorption. International Journal of Greenhouse Gas Control, 2010. 4: 771-775.

BEIS Committee Report, (2019). Carbon Capture usage and storage: Third time lucky, Twentieth report of Session 2017-19, 25th April 2019.

Cheng H., Lai C., Tan C. (2013). Thermal regeneration of alkanolamine solutions in a rotating packed bed. Int J Greenhouse Gas Control 16: 206–16.

Clean Growth, (2018). The UK Carbon Capture Usage and Storage deployment pathway-An action Plan, 2018.

Da Silva, E.F., Lepaumier, H., Grimstvedt, A., Vevelstad, S.J., Einbu, A., Vernstad, K., Svendsen, H.F., Zahlsen, K., (2012). Understanding 2-Ethanolamine Degradation in Postcombustion CO_2 Capture. Ind. Eng. Chem. Res. 2012, 51, 13329–13338.

de Cazenove T., Bouma RHB., Goetheer ELV., van Os PJ. and Hamborg ES., (2016). "Aerosol measurement technique: Demonstration at CO_2 Technology Centre Mongstad." Energy Proc 86:160–170.

Diego ME., Akram M., Bellas JM., Finney KN. and Pourkashanian M. (2017). Making gas-CCS a commercial reality: The challenges of scaling up. Greenhouse Gases: Science and Technology 7 (5): 778-807.

Einbu, A., Ciftja, A. F., Grimstvedt, A., Zakeri, A., & Svendsen, H. F. (2012). Online analysis of amine concentration and CO_2 loading in MEA solutions by ATR-FTIR spectroscopy. Energy Procedia, 23, 55-63. https://doi.org/10.1016/j.egypro.2012.06.040

Esbensen, K. H., Guyot, D., Westad, F., Houmoller, L.P. (2010). Multivariate data analysis: in practice: CAMO Software

Flø, N. E., Faramarzi, L., de Cazenove, T., Hvidsten, O. A., Morken, A. K., Hamborg, E. S., Gjernes, E. (2017). Results from MEA Degradation and Reclaiming Processes at the CO_2 Technology Centre Mongstad. Energy Procedia, 114, 1307-1324. https://doi.org/10.1016/j.egypro.2017.03.1899

Hakka, L., (2007). Cansolv Technologies Inc. 2007, private communication.

Herraiz L., (2016). Selective Exhaust Gas Recirculation in Combined Cycle Gas Turbine Power Plants with Post-combustion Carbon Capture. PhD Thesis. University of Edinburgh, Scotland, UK.

Idris, Z., Jens, K. J., & Eimer, D. A. (2014). Speciation of MEA-CO_2 Adducts at Equilibrium Using Raman Spectroscopy. Energy Procedia, 63, 1424-1431. https://doi.org/10.1016/j.egypro.2014.11.152

Jassim, M.S., Rochelle G., Eimer D. and Ramshaw C., (2007). Carbon dioxide absorption and desorption in aqueous monoethanolamine solutions in a rotating packed bed. Industrial & Engineering Chemistry Research, 2007. 46: 2823-2833.

Jinadasa, M. H. W. N. (2019). Process analytical technology for real-time quantitative speciation of aqueous phase CO_2 capture solvents. (PhD thesis), University of South-Eastern Norway, Porsgrunn. (ISBN: 978-82-7206-523-1)

Jinadasa, M. H. W. N., Jens, K.-J., & Halstensen, M. (2018). Process Analytical Technology for CO_2 Capture. In Karamé, I., Shaya, J., & Srour, H. (Eds.), Carbon Dioxide Chemistry, Capture and Oil Recovery: Intech Open. DOI: 10.5772/intechopen.76176

Jinadasa, M. H. W. N., Jens, K.-J., Øi, L. E., & Halstensen, M. (2017). Raman spectroscopy as an online monitoring tool for CO_2 capture process: Demonstration using a laboratory rig. Energy Procedia, 114, 1179-1194. https://doi.org/10.1016/j.egypro.2017.03.1282

Kachko, A. (2016). In-line monitoring of solvents during CO_2 absorption using multivariate data analysis. (PhD thesis), Technische Universiteit Delft, (ISBN: 978-94-6186-673-8)

Kachko, A., van der Ham, L. V., Bakker, D. E., van de Runstraat, A., Nienoord, M., Vlugt, T. J. H., & Goetheer, E. L. V. (2016a). In-Line Monitoring of the CO_2, MDEA, and PZ Concentrations in the Liquid Phase during High Pressure CO_2 Absorption. Industrial & Engineering Chemistry Research, 55(13), 3804-3812. 10.1021/acs.iecr.6b00141

797 Kachko, A., van der Ham, L. V., Bardow, A., Vlugt, T. J. H., & Goetheer, E. L. V. (2016b).
798 Comparison of Raman, NIR, and ATR FTIR spectroscopy as analytical tools for in-line
799 monitoring of CO_2 concentration in an amine gas treating process. International Journal of
800 Greenhouse Gas Control, 47, 17-24. https://doi.org/10.1016/j.ijggc.2016.01.020

801 Kachko, A., van der Ham, L. V., Geers, L. F. G., Huizinga, A., Rieder, A., Abu-Zahra, M.
802 R. M., Goetheer, E. L. V. (2015). Real-Time Process Monitoring of CO_2 Capture by
803 Aqueous AMP-PZ Using Chemometrics: Pilot Plant Demonstration. Industrial &
804 Engineering Chemistry Research, 54(21), 5769-5776. 10.1021/acs.iecr.5b00691

805 Kang J.L., Wong D.S.H., Jang S.S., and Tan C.S., (2016). A comparison between packed
806 beds and rotating packed beds for CO_2 capture using monoethanolamine and dilute aqueous
807 ammonia solutions. International Journal of Greenhouse Gas Control, 2016. 46: 228-239.

808 Kim, Y.E., Lim, J.A., Jeong, S.K., Yoon, Y.I., Bae, S.T., Nam, S.C., (2013). Comparison
809 of carbon dioxide absorption in aqueous MEA, DEA, TEA and AMP solutions. Bulletin of
810 Korean Chemical Society 34: 783–787.

811 Knudsen, J.N., Jensen, J.N., Vilhelmsen, P.J., Biede, O., (2007). First year operation
812 experience with a 1 t/h CO_2 absorption pilot plant at Esbjerg coal-fired power plant. In
813 Proceedings of the European Congress of Chemical Engineering (ECCE-6), Copenhagen,
814 Denmark, 16–20 September 2007.

815 Kohl, A.L., Nielsen, R.B., (1997). Gas Purification, 5th ed.; Gulf Professional Publishing:
816 Houston, TX, USA, 1997.

817 Kumar, S., Cho J.H. and Moon I., Ionic liquid-amine blends and CO_2 BOLs (2014).
818 Prospective solvents for natural gas sweetening and CO_2 capture technology – A review.
819 International Journal of Greenhouse Gas Control, 2014. 20: 87-116.

820 Le Moullec Y., Neveux T., Al Azki A., Chikukwa A. and Hoff KA., (2014). Process
821 modifications for solvent-based post-combustion CO_2 capture. Int J Greenhouse Gas
822 Control 31: 96–112.

823 Lepaumier, H., Da Silva, E.F., Einbu, A., Grimstvedt, A., Knudsen, J.N., Zahlsen, K.,
824 Svendsen, H.F., (2011). Comparison of MEA degradation in pilot-scale with lab-scale
825 experiments. Energy Procedia 2011, 4, 1652–1659.

826 Madan, T., Sachde, D., Lin, Y.-J., Frailie, P., Rochelle, G.T., (2013). Improved process
827 configurations for amine scrubbing. In: 7th Trondheim Conference on CO_2 Capture,
828 Transport and Storage, Trondheim (NO), 4–6 June.

829 Mejdell T. Vassbotn T. Juliussen O., et al. (2011). "Novel full height pilot plant for solvent
830 development and model validation." Energy Procedia 4:1753–1760.

831 Merkel TC. Wei X., He Z., White LS. Wijmans JG. Baker RW. (2013). Selective exhaust
832 gas recycle with membranes for CO_2 capture from natural gas combined cycle power plants.
833 Ind Eng Chem Res 52:1150–1159 (2013).

834 Montañés, R. M., Flø, N. E., Dutta, R., Nord, L. O., & Bolland, O. (2017). Dynamic Process
835 Model Development and Validation with Transient Plant Data Collected from an MEA Test

836 Campaign at the CO_2 Technology Center Mongstad. Energy Procedia, 114, 1538-1550.
837 https://doi.org/10.1016/j.egypro.2017.03.1284

838 Notz R, Mangalapally HP. and Hasse H. (2012). "Post combustion CO_2 capture by reactive
839 absorption: Pilot plant description and results of systematic studies with MEA." Int J
840 Greenhouse Gas Control 6: 84–112.

841 Oh SY. Yun S. Kim JK. (2018). Process integration and design for maximizing energy
842 efficiency of a coal fired power plant integrated with amine-based CO_2 capture process.
843 Applied Energy 216:311–322.

844 Polasek, J. and Bullin J.A., (2006). Selecting Amines for Sweetening Units, Bryan Research
845 and Engineering, Inc. - Technical Papers, 2006.

846 Puxty, G., Bennett, R., Conway, W., & Maher, D. (2016). A comparison of Raman and IR
847 spectroscopies for the monitoring and evaluation of absorbent composition during CO_2
848 absorption processes. International Journal of Greenhouse Gas Control, 49, 281-289.
849 https://doi.org/10.1016/j.ijggc.2016.03.012

850 Reynolds, A. J., Verheyen, T. V., Adeloju, S. B., Chaffee, A. L., & Meuleman, E. (2015).
851 Evaluation of methods for monitoring MEA degradation during pilot scale post-combustion
852 capture of CO_2. International Journal of Greenhouse Gas Control, 39, 407-419.
853 https://doi.org/10.1016/j.ijggc.2015.06.001

854 Rochelle, G.T., (2012). Thermal degradation of amines for CO_2 capture. Curr. Opin. Chem.
855 Eng. 2012, 1, 183–190.

856 Sachde, D., & Rochelle, G. T., (2014). Absorber Intercooling Configurations using
857 Aqueous Piperazine for Capture from Sources with 4 to 27% CO_2. Energy Procedia, 63,
858 1637-1656. https://doi.org/10.1016/j.egypro.2014.11.174

859 Souchon, V., Aleixo, M. d. O., Delpoux, O., Sagnard, C., Mougin, P., Wender, A., &
860 Raynal, L. (2011). In situ determination of species distribution in alkanolamine- H_2O-CO_2
861 systems by Raman spectroscopy. Energy Procedia, 4, 554-561.

862 Tait, P., Buschle, B., Milkowski, K., Akram, M., Pourkashanian, M., & Lucquiaud, M.
863 (2018). Flexible operation of post-combustion CO_2 capture at pilot scale with demonstration
864 of capture-efficiency control using online solvent measurements. International Journal of
865 Greenhouse Gas Control, 71, 253-277. https://doi.org/10.1016/j.ijggc.2018.02.023

866 Van der Ham, L.V., van Eckeveld, A.C., & Goetheer, E.L.V., (2014). Online Monitoring
867 of Dissolved CO_2 and MEA Concentrations: Effect of Solvent Degradation on Predictive
868 Accuracy. Energy Procedia, 63, 1223-1228. https://doi.org/10.1016/j.egypro.2014.11.132

869 Vogt, M., Pasel, C., & Bathen, D. (2011). Characterisation of CO_2 absorption in various
870 solvents for PCC applications by Raman spectroscopy. Energy Procedia, 4, 1520-1525.
871 https://doi.org/10.1016/j.egypro.2011.02.020

872 Wang M., Joel AS., Ramshaw C., Eimer D., Musa NM. (2015). Process intensification for
873 post-combustion CO_2 capture with chemical absorption: A critical review. Applied Energy
874 158: 275–291.

875 Wong, M. K., Shariff, A. M., & Bustam, M. A. (2015). Chemical speciation of CO_2
876 absorption in aqueous monoethanolamine investigated by in situ Raman spectroscopy.
877 International Journal of Greenhouse Gas Control, 39, 139–147.
878 https://doi.org/10.1016/j.ijggc.2015.05.016

879 Wong, M. K., Shariff, A. M., & Bustam, M. A. (2016). Raman spectroscopic study on the
880 equilibrium of carbon dioxide in aqueous monoethanolamine. RSC Advances, 6(13),
881 10816-10823. 10.1039/C5RA22926J

882 Xie, H.-B., Zhou, Y., Zhang, Y., & Johnson, J. K. (2010). Reaction Mechanism of
883 Monoethanolamine with CO_2 in Aqueous Solution from Molecular Modeling. The Journal
884 of Physical Chemistry A, 114(43), 11844-11852. 10.1021/jp107516k

885 Yang Q., Puxty G., James S., Bown M., Feron P., Conway W., (2016). Toward Intelligent
886 CO_2 Capture Solvent Design through Experimental Solvent Development and Amine
887 Synthesis. Energy Fuels 30: 7503−7510.

888 Yuan Y. and Rochelle G.T., (2018). CO_2 absorption rate in semi-aqueous
889 monoethanolamine. Chemical Engineering Science, 2018. 182: 56-66.

890

891

892